Acta Mech 226, 3333–3374 (2015)
DOI 10.1007/s00707-015-1374-7

ORIGINAL PAPER

Aysegul Kucuksucu · Mehmet A. Guler · Ahmet Avci

Mechanics of sliding frictional contact for a graded orthotropic half-plane

Received: 18 January 2015 / Revised: 14 April 2015 / Published online: 9 June 2015

Abstract The main interest in this study is the crack initiation in graded orthotropic materials under sliding contact conditions. We consider the two-dimensional sliding contact problem between a graded orthotropic half-plane and a rigid punch with an arbitrary profile. The orthotropic graded half-plane is modeled as a linearly elastic and locally inhomogeneous orthotropic material with an exponentially varying Young's modulus in the depth direction. The principal axes of orthotropy are assumed to be parallel and perpendicular to the contact surface. The problem is formulated under plane strain or generalized plane stress conditions. Using the standard Fourier transform, the problem is reduced to a singular integral equation, which is solved numerically using Jacobi polynomials. Extensive parametric study is done to determine the effect of the inhomogeneity parameter, β, the friction coefficient between the half-plane and the stamp, η, as well as the material orthotropic elastic parameters: the stiffness ratio, δ, the effective Poisson's ratio, ν, and the shear parameter, κ, on the contact stress distribution and stress intensity factors at the sharp edges of the stamps that may have a bearing on the fatigue and fracture of the graded orthotropic half-plane.

1 Introduction

Load-bearing components are common in many engineering applications such as cylinder linings, brake disks, disk dovetail connections, and abradable seals used in gas turbine components. The mating parts are usually subjected to high contact stresses that may result in wear and fatigue of the components and ultimately lead to the fracture of the machine elements. In these components, the substrate is usually coated with protective coatings in order to reduce wear and increase fatigue life of the parts. The base material used in most of these high-temperature applications is generally ceramic, and the state of the contact in the contact zone is frictional. Possessing low fracture toughness, ceramics have some shortcomings such as being brittle and susceptible to surface cracking and spallation. Lately, functionally graded materials (FGMs) have been proposed to alleviate

A. Kucuksucu
Department of Mechanical Engineering, Bursa Orhangazi University, Bursa 16310, Turkey
E-mail: aysegul.kucuksucu@bou.edu.tr; a.kucuksucu@etu.edu.tr
Tel.: +90-4448268

A. Kucuksucu · M. A. Guler (✉)
Department of Mechanical Engineering, TOBB University of Economics and Technology, Ankara 06560, Turkey
E-mail: mguler@etu.edu.tr; prof.guler@gmail.com
Tel.: +90-312-2924088

A. Avci
Department of Mechanical Engineering, Selçuk University, Konya 42003, Turkey
E-mail: aavci@selcuk.edu.tr
Tel.: +90-332-2231907

some of the mentioned problems and to improve the tribological performance of the mating components. FGMs are generally two phase composites possessing smooth spatial variations in the volume fractions of the constituents.

Fatigue life assessment of the load-bearing components requires a complete understanding of the contact stresses that may be responsible for components failure. Contact mechanics plays a crucial role in these situations, and it is well established for structural components having homogeneous and isotropic material properties [1–9]. The reader is referred to the review paper by Barber and Ciavarella [10] for an extensive survey about contact mechanics problems. For the contact mechanics of graded materials or FGMs, the readers are referred to [11–18]. Contact mechanics of FGMs with finite size is considerably different than the ones with the infinite graded models. For example, a thermo-mechanical sliding contact problem for a finite graded layer and a partial slip contact for an elastic graded solid with finite thickness are studied by Chen and Chen [19,20], respectively. Note that, the medium is assumed to be isotropic in all mentioned studies, whereas in this study the contacting half-plane is taken to be graded orthotropic.

In all of the studies about contact mechanics of FGMs mentioned above, interface adhesion is not considered. However, there are also contact mechanics models where interface adhesion is included. Giannakopoulos and Pallot [21] considered two-dimensional plane strain adhesive contact model. For the mechanics of adhesive contact of power-law graded materials, the readers are referred to [22,23].

Several studies have been conducted for the contact mechanics of transversely isotropic materials [24–29]. There are some studies that solve the contact problem using an analogy to the crack problems [30], using Green's functions [31–33] or method of integral characteristics of solutions to the boundary-initial value problems [34]. Using the Fourier expansion of the Green's function for the frictionless normal contact problem, Ciavarella et al. [35] presented a method for solving 3D contact problem between generally anisotropic materials with any second-order surface geometry. The Green's function used in their method required using the Barnett–Lothe method [36]. Shi et al. [37] solved the frictionless contact problem of a rigid ellipsoid indenting an orthotropic half-plane, with the surface of the half-plane parallel to two of the axes of material symmetry. Swanson [38] combined two previous solution techniques [39–41] in order to calculate the stresses due to the contact loading in orthotropic materials. Lin and Ovaert [42] studied the two-dimensional frictional isothermal rough surface contact problem of the general anisotropic materials. The applications of analytical methods in the solutions of boundary value problems (BVPs) for anisotropic elasticity are given in the monograph by Rand and Rovenskii [43]. Ning et al. [44] focused on the axisymmetric indentation of a rigid, frictionless sphere into a transversely isotropic layer. Li and Wang [45] studied the Hertzian contact of anisotropic piezoelectric bodies. Ramirez [46] analyzed the response of an arbitrarily multilayered piezoelectric half-plane indented by a rigid frictionless parabolic punch. Galin's [47] original work in 1953 about the contact problems of an anisotropic half-plane is translated into English in 2008 and mainly covers the methods developed by Muskhelishvili [3]. He and Ovaert [48] formulated the three-dimensional rough surface contact problem for a semi-infinite anisotropic elastic half-plane in contact with a rough, rigid sphere by applying the line integral of Barnett–Lothe tensors on oblique planes. Batra and Jiang [49], and Jiang and Batra [50] used the Stroh formalism to study analytically the generalized plane strain deformations of a linear elastic anisotropic layer and two-layer elastic composite with a through-the-width rectangular void between them, respectively. Erbas et al. [51] investigated the frictionless contact of a punch with an elastic strip. The two-dimensional frictionless sliding contact over orthotropic piezoelectric medium indented by a rigid sliding punch was investigated by Zhou and Lee [52]. Using semi-analytical methods, Bagault et al. [53,54] studied the effect of anisotropy orientation on the contact solution of an anisotropic half space indented by a rigid sphere. The boundary element method (BEM) was also used to solve the generalized plane contact problems of the anisotropic materials with possible friction contact zones [55,56] (see Blazquez et al. [55] for 2D and Rodríguez-Tembleque et al. [56] for 3D). Recently, Guler [57] provided a closed-form solution to the two-dimensional frictional contact problem of a homogeneous orthotropic medium in contact with a sliding rigid stamp. In fact, this study is an extension of the problem solved by Guler [57] and Kucuksucu et al. [58].

Concerning the literature on the contact mechanics of graded orthotropic or inhomogeneous medium, the only closest study is the frictionless contact problem of a rigid stamp on an elastic orthotropic half-plane considered by Bakırtaş [59]. He formulated the problem using the Fourier transform technique and solved the resultant Fredholm integral equation of the first type. To the best of the author's knowledge, two-dimensional frictional contact problem of a rigid stamp on a graded orthotropic half-plane has not been solved in the open literature. The present study provides the analytical solution of the contact stresses in terms of the orthotropic material parameters, the coefficient of friction, and the spatial coordinates. The strength of the singularities

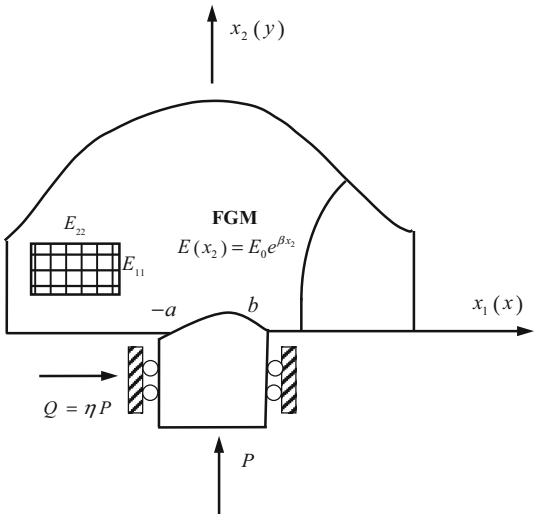

Fig. 1 Geometry of the sliding frictional contact problem for graded orthotropic half-plane

and the stress intensity factors at both ends of the flat stamp are also found in terms of the orthotropic material parameters and the coefficient of friction.

The problem under consideration consists of the sliding contact between a graded orthotropic elastic half-plane and a rigid stamp subjected to the external loads P and Q (see Fig. 1). The mixed boundary value problem is formulated analytically using the Fourier transform technique. The resultant Fredholm integral equation of the second type is solved numerically using Jacobi polynomials. Therefore, the objective of the study was to obtain a series of analytical benchmark solutions for examining the influence of material orthotropy and the coefficient of friction on the critical stresses that may have a bearing on the fatigue and fracture of the graded orthotropic half-plane.

This paper is organized as follows. The problem description and formulation are provided in Sect. 2. The integral equation of the problem is detailed in Sect. 3. The analytical solution of the problem is given in Sect. 4. The in-plane stress derivation is presented in Sect. 5. The solution of the contact problem for a flat and wedge stamp is outlined in Sect. 6. The numerical results are then discussed in Sect. 7. Finally, concluding remarks are given in Sect. 8.

2 Formulation of the contact problem

The geometry of the two-dimensional sliding frictional contact problem between an elastic graded orthotropic half-plane and a rigid stamp is depicted in Fig. 1. The Cartesian coordinate system is intentionally selected in such a way that the principal axes of orthotropy are aligned with the (x_1, x_2) coordinate system. The contact surface extends from $x_1 = -a$ to $x_1 = b$ at $x_2 = 0$. The magnitudes of the normal and tangential forces acting on the stamp are represented by P and Q, respectively. It is assumed that Coulomb's dry friction law governs the sliding frictional contact problem. Thus, the relation between P and Q can be expressed as $Q = \eta P$, where η is the coefficient of static friction. In the contact problem considered, u_i and σ_{ij} $(i, j = 1, 2)$ denote the displacement and stress components and E_{ii}, G_{ij} and ν_{ij} $(i, j = 1, 2, 3)$ denote engineering elastic parameters, respectively. We now introduce the following definitions in order to replace four independent engineering constants E_{11}, E_{22}, G_{12}, and ν_{12} by four elastic parameters, namely the effective stiffness (E), the effective Poisson's ratio (ν), the stiffness ratio (δ), and the shear parameter (κ) [60,61]:

$$E = \sqrt{E_{11}E_{22}}, \quad \nu = \sqrt{\nu_{12}\nu_{21}}, \quad \delta^4 = \frac{E_{11}}{E_{22}} = \frac{\nu_{12}}{\nu_{21}}, \quad \kappa = \frac{E}{2G_{12}} - \nu, \tag{1a–d}$$

for generalized plane stress conditions. For plane strain conditions, Eq. (1) must be replaced by:

$$E = \sqrt{\frac{E_{11}E_{22}}{(1-\nu_{13}\nu_{31})(1-\nu_{23}\nu_{32})}}, \quad \nu = \sqrt{\frac{(\nu_{12}+\nu_{13}\nu_{32})(\nu_{21}+\nu_{23}\nu_{31})}{(1-\nu_{13}\nu_{31})(1-\nu_{23}\nu_{32})}}, \tag{2a,b}$$

$$\delta^4 = \frac{E_{11}}{E_{22}} \frac{1-\nu_{23}\nu_{32}}{1-\nu_{13}\nu_{31}}, \quad \kappa = \frac{E}{2G_{12}} - \nu. \tag{2c, d}$$

Using the aforementioned parameters, the relationship between the strain and the stress components can be expressed as:

$$\begin{bmatrix} \varepsilon_{11} \\ \varepsilon_{22} \\ 2\varepsilon_{12} \end{bmatrix} = \frac{1}{E(x_1, x_2)} \begin{bmatrix} \delta^{-2} & -\nu & 0 \\ -\nu & \delta^2 & 0 \\ 0 & 0 & 2(\kappa+\nu) \end{bmatrix} \begin{bmatrix} \sigma_{11} \\ \sigma_{22} \\ \sigma_{12} \end{bmatrix}. \tag{3}$$

Note that, the elasticity matrix is symmetric $(\nu_{ij}/E_{ii}) = (\nu_{ji}/E_{jj})$. We use the following transformation from the physical coordinate system (x_1, x_2) to transformed coordinate system (x, y) by using the parameter δ as a scaling constant:

$$x = \frac{x_1}{\sqrt{\delta}}, \quad y = x_2\sqrt{\delta}, \tag{4a–b}$$

$$u(x, y) = \sqrt{\delta}u_1(x_1, x_2), \quad v(x, y) = \frac{1}{\sqrt{\delta}}u_2(x_1, x_2), \tag{4c–d}$$

$$\sigma_{xx}(x, y) = \sigma_{11}(x_1, x_2)/\delta, \quad \sigma_{yy}(x, y) = \delta\sigma_{22}(x_1, x_2), \tag{4e–f}$$

$$\sigma_{xy}(x, y) = \sigma_{12}(x_1, x_2). \tag{4g}$$

Using Eqs. (4), the stress–displacement relations in the (x, y) coordinate system become

$$\sigma_{xx}(x, y) = \frac{E^*(x, y)}{1-\nu^2}\left\{\frac{\partial u(x, y)}{\partial x} + \nu\frac{\partial v(x, y)}{\partial y}\right\}, \tag{5a}$$

$$\sigma_{yy}(x, y) = \frac{E^*(x, y)}{1-\nu^2}\left\{\nu\frac{\partial u(x, y)}{\partial x} + \frac{\partial v(x, y)}{\partial y}\right\}, \tag{5b}$$

$$\sigma_{xy}(x, y) = \frac{E^*(x, y)}{2(\kappa+\nu)}\left\{\frac{\partial u(x, y)}{\partial y} + \frac{\partial v(x, y)}{\partial x}\right\}, \tag{5c}$$

where

$$E^*(x, y) = E(x_1, x_2). \tag{6}$$

The governing partial differential equations for the two-dimensional plane contact problem under consideration can be found using a displacement-based formulation. By substituting Eqs. (5) into equations of equilibrium, $\sigma_{ij,j} = 0$, $(i, j = 1, 2)$, we obtain:

$$\frac{\partial^2 u}{\partial y^2} + \beta_1\frac{\partial^2 u}{\partial x^2} + \beta_2\frac{\partial^2 v}{\partial x\partial y} + \frac{1}{E^*}\left[\beta_1\frac{\partial E^*}{\partial x}\left(\frac{\partial u}{\partial x} + \nu\frac{\partial v}{\partial y}\right) + \frac{\partial E^*}{\partial y}\left(\frac{\partial u}{\partial y} + \frac{\partial v}{\partial x}\right)\right] = 0, \tag{7a}$$

$$\frac{\partial^2 v}{\partial x^2} + \beta_1\frac{\partial^2 v}{\partial y^2} + \beta_2\frac{\partial^2 u}{\partial x\partial y} + \frac{1}{E^*}\left[\frac{\partial E^*}{\partial x}\left(\frac{\partial u}{\partial y} + \frac{\partial v}{\partial x}\right) + \beta_1\frac{\partial E^*}{\partial y}\left(\frac{\partial v}{\partial y} + \nu\frac{\partial u}{\partial x}\right)\right] = 0, \tag{7b}$$

where

$$\beta_1 = \frac{2(\kappa+\nu)}{1-\nu^2}, \quad \beta_2 = 1 + \nu\beta_1. \tag{8a,b}$$

In this study, it is assumed that the material properties vary only in x_2-direction. Therefore, the graded half-plane can be approximated by defining the function $E(x_1, x_2)$:

$$E(x_1, x_2) = E(x_2) = E_0 e^{\beta x_2} = E^*(x, y) = E_0^* e^{\gamma y},$$
$$\gamma = \frac{\beta}{\sqrt{\delta}},$$
$$E_0^* = \begin{cases} E_0, & \text{generalized plane stress conditions,} \\ \frac{E_0}{1-\nu_0^2}, & \text{plane strain conditions,} \end{cases} \tag{9a–c}$$

where β is the constant defining the material inhomogeneity in the physical coordinate system (x_1, x_2) with a dimension of [Length^{-1}]. Herein we use the dimensionless parameters βa and βb for the flat and wedge stamps, respectively.
The governing system of equations can be found by substituting Eqs. (9) into Eqs. (7):

$$\frac{\partial^2 u}{\partial y^2} + \beta_1 \frac{\partial^2 u}{\partial x^2} + \beta_2 \frac{\partial^2 v}{\partial x \partial y} + \gamma \left(\frac{\partial u}{\partial y} + \frac{\partial v}{\partial x} \right) = 0, \tag{10a}$$

$$\frac{\partial^2 v}{\partial x^2} + \beta_1 \frac{\partial^2 v}{\partial y^2} + \beta_2 \frac{\partial^2 u}{\partial x \partial y} + \beta_1 \gamma \left(\frac{\partial v}{\partial y} + \nu \frac{\partial u}{\partial x} \right) = 0. \tag{10b}$$

Note that when the material inhomogeneity parameter in the transformed coordinate system $\gamma = 0$, we obtain the corresponding equations for an orthotropic homogeneous half-plane (see [57,58]).

The general solution of the governing field equations can be obtained by applying Fourier transformation in x-direction. The expressions for the displacement and stress components become

$$u(x, y) = \frac{1}{2\pi} \int_{-\infty}^{\infty} F(\alpha, y) \mathrm{e}^{i\alpha x} \mathrm{d}\alpha, \tag{11a}$$

$$v(x, y) = \frac{1}{2\pi} \int_{-\infty}^{\infty} G(\alpha, y) \mathrm{e}^{i\alpha x} \mathrm{d}\alpha, \tag{11b}$$

$$\sigma_{xx}(x, y) = \frac{E_0^* \mathrm{e}^{\gamma y}}{1 - \nu^2} \frac{1}{2\pi} \left\{ \int_{-\infty}^{\infty} \left[i\alpha F(\alpha, y) + \nu \frac{\mathrm{d}G}{\mathrm{d}y}(\alpha, y) \right] \mathrm{e}^{i\alpha x} \mathrm{d}\alpha \right\}, \tag{12a}$$

$$\sigma_{yy}(x, y) = \frac{E_0^* \mathrm{e}^{\gamma y}}{1 - \nu^2} \frac{1}{2\pi} \left\{ \int_{-\infty}^{\infty} \left[i\alpha \nu F(\alpha, y) + \frac{\mathrm{d}G}{\mathrm{d}y}(\alpha, y) \right] \mathrm{e}^{i\alpha x} \mathrm{d}\alpha \right\}, \tag{12b}$$

$$\sigma_{xy}(x, y) = \frac{E_0^* \mathrm{e}^{\gamma y}}{2(\kappa + \nu)} \frac{1}{2\pi} \left\{ \int_{-\infty}^{\infty} \left[\frac{\mathrm{d}F}{\mathrm{d}y}(\alpha, y) + i\alpha G(\alpha, y) \right] \mathrm{e}^{i\alpha x} \mathrm{d}\alpha \right\}, \tag{12c}$$

$$F(\alpha, y) = \sum_{j=1}^{4} C_j(\alpha) \mathrm{e}^{n_j y}, \quad G(\alpha, y) = \sum_{j=1}^{4} D_j(\alpha) \mathrm{e}^{n_j y}, \tag{13a,b}$$

where α is the transform variable, $i^2 = -1$, $C_j(\alpha)$, $D_j(\alpha)$ $(j = 1, \ldots, 4)$ are arbitrary unknowns and $n_j(\alpha)$ $(j = 1, \ldots, 4)$ are the roots of the following characteristic equation:

$$\left(n^2 + \gamma n - \kappa \alpha^2 - i\,|\alpha|\,\delta_1 \right) \left(n^2 + \gamma n - \kappa \alpha^2 + i\,|\alpha|\,\delta_1 \right) = 0, \tag{14}$$

where

$$\delta_1 = \sqrt{\nu \gamma^2 + \left(1 - \kappa^2\right) \alpha^2}. \tag{15}$$

The roots of the characteristic Eq. (14) are dependent on the value of κ and are given in Appendix A.

In the formulation given above, there are a total of eight unknowns $C_j(\alpha)$ and $D_j(\alpha)$ $(j = 1, \ldots, 4)$ which are not independent. The relationship between them can be written as

$$C_j(\alpha) = A_j D_j(\alpha), \quad j = 1, 2, \tag{16a}$$

$$C_j(\alpha) = -\overline{A_j} D_j(\alpha), \quad j = 3, 4. \tag{16b}$$

where

$$A_j(\alpha) = \frac{(\beta_1 \kappa - 1)\,\alpha^2 + i\beta_1\,|\alpha|\,\delta_1}{-i\alpha \left(\beta_2 n_j + \beta_1 \gamma \nu \right)}. \tag{17}$$

One can observe that the stresses and displacements should be bounded as $\left|x_1^2 + x_2^2\right| \to \infty$. This regularity condition requires that the only admissible roots are the ones with $\Re e\left(n_j\right) < 0\,(j = 2, 4)$ and therefore the functions $C_j(\alpha) = D_j(\alpha) = 0\ \ (j = 1, 3)$. Finally, Eq. (13) becomes

$$F(\alpha, y) = A_2 D_2(\alpha) \mathrm{e}^{n_2 y} - \overline{A_2} D_4(\alpha) \mathrm{e}^{\overline{n_2} y}, \tag{18a}$$

$$G(\alpha, y) = D_2(\alpha) \mathrm{e}^{n_2 y} + D_4(\alpha) \mathrm{e}^{\overline{n_2} y}. \tag{18b}$$

The remaining two unknowns $D_2(\alpha)$ and $D_4(\alpha)$ are obtained in terms of the boundary tractions in the transformed domain (see Fig. 2). That is:

$$D_2(\alpha) = -\frac{1}{E_0^* \Delta_0(\alpha)} \left[\left(1 - \nu^2\right) \bar{Z}_2(\alpha) P(\alpha) + 2\left(\kappa + \nu\right) \bar{Z}_1(\alpha) Q(\alpha)\right], \tag{19a}$$

$$D_4(\alpha) = \frac{1}{E_0^* \Delta_0(\alpha)} \left[2\left(\kappa + \nu\right) Z_1(\alpha) Q(\alpha) - \left(1 - \nu^2\right) Z_2(\alpha) P(\alpha)\right], \tag{19b}$$

where we have defined:

$$Z_1(\alpha) = n_2 + i\alpha\nu A_2(\alpha), \tag{20a}$$

$$Z_2(\alpha) = A_2(\alpha) n_2 + i\alpha, \tag{20b}$$

$$\Delta_0(\alpha) = -\left[Z_1(\alpha) \bar{Z}_2(\alpha) + \bar{Z}_1(\alpha) Z_2(\alpha)\right], \tag{20c}$$

$$P(\alpha) = \int_{-\infty}^{\infty} \sigma_{yy}\,(t, 0)\, \mathrm{e}^{-i\alpha t} \mathrm{d}t, \tag{20d}$$

$$Q(\alpha) = \int_{-\infty}^{\infty} \sigma_{xy}\,(t, 0)\, \mathrm{e}^{-i\alpha t} \mathrm{d}t. \tag{20e}$$

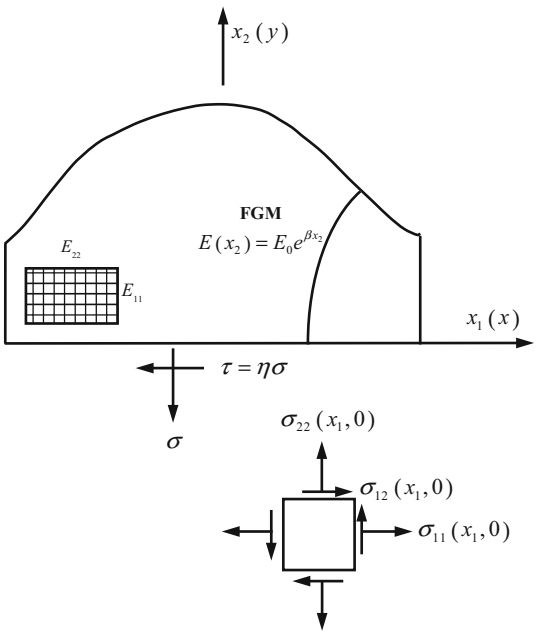

Fig. 2 Geometry of the plane contact problem for graded orthotropic half-plane for the plane stress case

3 The integral equation of the problem

The singular integral equations of the problem can be obtained after some length algebraic manipulations (see Appendix B and [62]) as:

$$-\omega_1\sigma_{xy}(x,0)-\frac{1}{\pi}\int\limits_{-a/\sqrt{\delta}}^{b/\sqrt{\delta}}\left[\frac{1}{t-x}-J_{11}(t,x)\right]\sigma_{yy}(t,0)\,\mathrm{d}t$$
$$+\frac{1}{\pi}\int\limits_{-a/\sqrt{\delta}}^{b/\sqrt{\delta}}J_{12}(t,x)\sigma_{xy}(t,0)\,\mathrm{d}t=\lambda_1E_0^*f(x), \tag{21a}$$

$$\omega_2\sigma_{yy}(x,0)-\frac{1}{\pi}\int\limits_{-a/\sqrt{\delta}}^{b/\sqrt{\delta}}\left[\frac{1}{t-x}-J_{22}(t,x)\right]\sigma_{xy}(t,0)\,\mathrm{d}t$$
$$+\frac{1}{\pi}\int\limits_{-a/\sqrt{\delta}}^{b/\sqrt{\delta}}J_{21}(t,x)\sigma_{yy}(t,0)\,\mathrm{d}t=\lambda_2E_0^*g(x), \tag{21b}$$

with

$$f(x)=\frac{\partial}{\partial x}v(x,0),\quad g(x)=\frac{\partial}{\partial x}u(x,0), \tag{22a,b}$$

where a_0, b_0, c_0, d_0 are given in Appendix B and $\omega_1, \omega_2, \lambda_1, \lambda_2, J_{ij}, \Phi_{ij}$, $(i, j = 1, 2)$ are given in Appendix C.

Note that for an orthotropic homogeneous half-plane where the inhomogeneity parameter is zero, i.e., $\gamma = 0$, the integral equation similar to (21a) and (21b) can be written in the form given in [57]. Observe that, since the axes orientations defining the problem geometry are different, the sign of the Cauchy integral is reversed. Guler [57] used the lower half-plane, whereas in this study, the upper half-plane is used as the contacting half-plane. Hence we recover:

$$-\omega_1^{\mathrm{ort}}\sigma_{xy}(x,0)-\frac{1}{\pi}\int\limits_{-a/\sqrt{\delta}}^{b/\sqrt{\delta}}\frac{\sigma_{yy}(t,0)}{t-x}\mathrm{d}t=\lambda_1^{\mathrm{ort}}E_0f(x),\quad -\frac{a}{\sqrt{\delta}}<x<\frac{b}{\sqrt{\delta}}, \tag{23a}$$

$$\omega_2^{\mathrm{ort}}\sigma_{yy}(x,0)-\frac{1}{\pi}\int\limits_{-a/\sqrt{\delta}}^{b/\sqrt{\delta}}\frac{\sigma_{xy}(t,0)}{t-x}\mathrm{d}t=\lambda_2^{\mathrm{ort}}E_0g(x),\quad -\frac{a}{\sqrt{\delta}}<x<\frac{b}{\sqrt{\delta}}, \tag{23b}$$

where ω_1^{ort}, ω_2^{ort}, λ_1^{ort}, λ_2^{ort} are the parameters corresponding to orthotropic homogeneous half-plane and they are given in [57]. Note that:

$$\lambda_1^{\mathrm{ort}}=\begin{cases}\lambda_1, & \text{generalized plane stress conditions,}\\ \frac{\lambda_1}{1-\nu_0^2}, & \text{plane strain conditions,}\end{cases} \tag{24a}$$

$$\lambda_2^{\mathrm{ort}}=\begin{cases}\lambda_2, & \text{generalized plane stress conditions,}\\ \frac{\lambda_2}{1-\nu_0^2}, & \text{plane strain conditions.}\end{cases} \tag{24b}$$

The expressions (21) constitute a pair of integral equations for the unknown contact stresses $\sigma_{yy}(x, 0)$ and $\sigma_{xy}(x, 0)$ provided the stamp profile, that is, $u_1(x_1, 0)$ and $u_2(x_1, 0)$, $-a < x_1 < b$ are prescribed.

For a complete solution of the problem, the following equilibrium equation has to be also satisfied at the contact surface:

$$\int_{-a}^{b} \sigma_{22}(t_1, 0)\mathrm{d}t_1 = P, \tag{25}$$

where P is the resultant compressive force. The amplitude of the applied load may be given in terms of either the load, P, or stamp displacement, u_2, parallel to the x_2 axis.

In this study, it is assumed that the stamp moves relative to the graded half-plane, the coefficient of friction η in the contact region is constant and Coulomb type of the friction holds. If the direction of the forces P and Q is taken as Fig. 1, boundary conditions become

$$\sigma_{22}(x_1, 0) = \begin{cases} -p(x_1), & -a < x_1 < b, \\ 0 & x_1 < -a, x_1 > b, \end{cases} \tag{26a}$$

$$\sigma_{12}(x_1, 0) = \begin{cases} -\eta p(x_1), & -a < x_1 < b, \\ 0 & x_1 < -a, x_1 > b. \end{cases} \tag{26b}$$

Equations (26a, 26b) can be written in the transformed coordinate system using the transformations defined in Eqs. (4a–e) as

$$\sigma_{yy}(x, 0) = \begin{cases} -\delta p(x), & -\frac{a}{\sqrt{\delta}} < x < \frac{b}{\sqrt{\delta}}, \\ 0 & x < \frac{-a}{\sqrt{\delta}}, x > \frac{b}{\sqrt{\delta}}, \end{cases} \tag{27a}$$

$$\sigma_{xy}(x, 0) = \begin{cases} -\eta p(x), & -\frac{a}{\sqrt{\delta}} < x < \frac{b}{\sqrt{\delta}}, \\ 0 & x < \frac{-a}{\sqrt{\delta}}, x > \frac{b}{\sqrt{\delta}}. \end{cases} \tag{27b}$$

Using Eqs. (27a, 27b), Eqs. (21) can be obtained as follows:

$$\omega_1 \eta p(x) + \frac{1}{\pi} \int_{-a/\sqrt{\delta}}^{b/\sqrt{\delta}} \left[\frac{\delta}{t - x} - \delta J_{11}(t, x) - \eta J_{12}(t, x) \right] p(t)\,\mathrm{d}t = \lambda_1 E_0^* f(x), \tag{28a}$$

$$-\omega_2 \delta p(x) + \frac{1}{\pi} \int_{-a/\sqrt{\delta}}^{b/\sqrt{\delta}} \left[\frac{\eta}{t - x} - \delta J_{21}(t, x) - \eta J_{22}(t, x) \right] p(t)\,\mathrm{d}t = \lambda_2 E_0^* g(x). \tag{28b}$$

In order to normalize the limits of the integrals appearing in Eqs. (28), the following change of variables is introduced:

$$x = \frac{b + a}{2\sqrt{\delta}} r + \frac{b - a}{2\sqrt{\delta}}, \quad t = \frac{b + a}{2\sqrt{\delta}} s + \frac{b - a}{2\sqrt{\delta}},$$
$$-\frac{a}{\sqrt{\delta}} < (x, t) < \frac{b}{\sqrt{\delta}}, \quad -1 < (r, s) < 1, \tag{29a,b}$$

$$p(x) = \lambda_1 E_0^* \phi(r), \quad f(x) = F(r),$$
$$A = \omega_1 \eta, \quad B = \delta. \tag{30a–d}$$

Finally, the singular integral equation of the contact problem can be written in terms of normalized variables:

$$A\phi(r) + \frac{B}{\pi} \int_{-1}^{1} \frac{\phi(s)}{s - r}\mathrm{d}s - \frac{1}{\pi} \int_{-1}^{1} \left[\delta J_{11}^*(s, r) + \eta J_{12}^*(s, r) \right] \phi(s)\mathrm{d}s = F(r),$$
$$-1 < r < 1, \tag{31}$$

where

$$J_{ij}^{*}(s,r)=\frac{b+a}{2\sqrt{\delta}}J_{ij}\,(t,x)\quad(i,j=1,2)\,, \tag{32}$$

4 On the solution of the integral equations

For an accurate and efficient solution of the integral equation, the corresponding weight function $w(s)$ needs to be determined. By defining the complex potential

$$\Phi(z)=\frac{1}{2\pi i}\int_{-1}^{1}\frac{\phi(s)}{s-z}\mathrm{d}s \tag{33}$$

and using the complex function theory [3] from the dominant part of the integral equation (31)

$$A\phi(r)+\frac{B}{\pi}\int_{-1}^{1}\frac{\phi(s)}{s-r}\mathrm{d}s=G(r),\quad -1<r<1, \tag{34}$$

the weight function of $\phi(s)$ may be determined as

$$w(s)=(1-s)^{\alpha}\,(1+s)^{\beta}\,,\quad -1<s<1, \tag{35}$$

$$\alpha=-\frac{\theta}{\pi}+N_0,\quad \beta=\frac{\theta}{\pi}+M_0,\quad \theta=\arctan\left|\frac{B}{A}\right|, \tag{36}$$

where N_0 and M_0 are arbitrary (positive, zero, or negative) integers depending on the physics of the problem. In Eq. (34), $G(r)$ represents all the bounded terms in Eq. (31) where A and B are defined in Eq. (30c, d). After determining $w(s)$, the solution of Eq. (31) may be expressed as

$$\phi(s)=\sum_{n=0}^{\infty}c_n w(s)P_n^{(\alpha,\beta)}(s),\quad -1<s<1, \tag{37}$$

where c_n are the unknown coefficients and $P_n^{(\alpha,\beta)}(s)$ are Jacobi polynomials associated with the weight function $w(s)$. The following property of Jacobi polynomials is utilized in solving the integral equation (31)

$$AP_n^{(\alpha,\beta)}(r)w(r)+\frac{B}{\pi}\int_{-1}^{1}\frac{P_n^{(\alpha,\beta)}(s)w(s)}{s-r}\mathrm{d}s=-2^{-\chi}\frac{B}{\sin\pi\alpha}P_{n-\chi}^{(-\alpha,-\beta)}(r),$$
$$-1<r<1,\quad \Re(\alpha)>1,\quad \Re\,(\beta)>1,\quad \Re(\alpha)\neq(0,1,\ldots,)\,, \tag{38}$$

where χ is the index of the integral equation [3,63] defined as

$$\chi=-(\alpha+\beta). \tag{39}$$

By substituting (37) into (31) and using (38), it can be shown that

$$\sum_{n=0}^{\infty}c_n\left[-2^{-\chi}\frac{\delta}{\sin\pi\alpha}P_{n-\chi}^{(-\alpha,-\beta)}(r)+h_n^1(r)+h_n^2(r)\right]=F(r),\quad -1<r<1, \tag{40}$$

$$h_n^1(r)=-\frac{\delta}{\pi}\int_{-1}^{1}J_{11}^{*}(s,r)P_n^{(\alpha,\beta)}(s)w(s)\mathrm{d}s, \tag{41}$$

$$h_n^2(r)=-\frac{\eta}{\pi}\int_{-1}^{1}J_{12}^{*}(s,r)P_n^{(\alpha,\beta)}(s)w(s)\mathrm{d}s. \tag{42}$$

Now, Eq. (40) can be reduced into a system of algebraic equations in terms of the unknown coefficients, c_n, through a suitable collocation technique [64]. Higher accuracy is obtained in the numerical solution of (40), if the density of the collocation points is increased near the ends by choosing the collocation points $(r_i, i = 0, 1, \ldots, N)$ as the roots of the Jacobi polynomials depending on the index of the problem.

5 The in-plane stress component on the surface of the orthotropic medium

From the crack initiation and surface damage point of view, one of the important components of the stress state at the surface of the medium is the in-plane stress component $\sigma_{11}(x_1, 0)$. When this component of the stress state at the surface becomes tensile, crack initiation or surface damage can occur especially at the trailing edge of the contact [12,18]. In this section, we briefly discuss the formulation and calculation of this stress component.

In the transformed domain (x, y), the Hooke's law for the surface stress components can be expressed using Eqs. (5):

$$\sigma_{xx}(x,0) = \frac{E_0^*}{1-\nu^2}\left\{\frac{\partial u(x,0)}{\partial x} + \nu\frac{\partial v(x,0)}{\partial y}\right\}, \tag{43a}$$

$$\sigma_{yy}(x,0) = \frac{E_0^*}{1-\nu^2}\left\{\nu\frac{\partial u(x,0)}{\partial x} + \frac{\partial v(x,0)}{\partial y}\right\}, \tag{43b}$$

$$\sigma_{xy}(x,0) = \frac{E_0^*}{2(\kappa+\nu)}\left\{\frac{\partial u(x,0)}{\partial y} + \frac{\partial v(x,0)}{\partial x}\right\}. \tag{43c}$$

Also, from Eqs. (21), (22), and (43b), one can find the displacement derivatives at the surface as given below:

$$\frac{\partial}{\partial x}u(x,0) = \frac{\omega_2}{\lambda_2 E_0^*}\sigma_{yy}(x,0) - \frac{1}{\pi\lambda_2 E_0^*}\int_{-a/\sqrt{\delta}}^{b/\sqrt{\delta}}\left[\frac{1}{t-x} - J_{22}(t,x)\right]\sigma_{xy}(t,0)\,\mathrm{d}t$$

$$+\frac{1}{\pi\lambda_2 E_0^*}\int_{-a/\sqrt{\delta}}^{b/\sqrt{\delta}} J_{21}(t,x)\sigma_{yy}(t,0)\,\mathrm{d}t, \tag{44a}$$

$$\frac{\partial v(x,0)}{\partial y} = \frac{1-\nu^2}{E_0^*}\sigma_{yy}(x,0) - \nu\frac{\partial u(x,0)}{\partial x}. \tag{44b}$$

Now, substituting Eqs. (44b) into Eq. (43a), it can be shown that

$$\sigma_{xx}(x,0) = E_0^*\frac{\partial u(x,0)}{\partial x} + \nu\sigma_{yy}(x,0). \tag{45}$$

Finally, substituting (44a) into (45), we have

$$\sigma_{xx}(x,0) = \sigma_{xx}^p(x,0) + \sigma_{xx}^q(x,0), \tag{46}$$

$$\sigma_{xx}^p(x,0) = \left(\frac{\omega_2}{\lambda_2} + \nu\right)\sigma_{yy}(x,0) + \frac{1}{\pi\lambda_2}\int_{-a/\sqrt{\delta}}^{b/\sqrt{\delta}} J_{21}(t,x)\sigma_{yy}(t,0)\,\mathrm{d}t, \tag{47a}$$

$$\sigma_{xx}^q(x,0) = -\frac{1}{\pi\lambda_2}\int_{-a/\sqrt{\delta}}^{b/\sqrt{\delta}}\left[\frac{1}{t-x} - J_{22}(t,x)\right]\sigma_{xy}(t,0)\,\mathrm{d}t. \tag{47b}$$

Or in the physical coordinate system, (x_1, x_2), the in-plane stress component can be expressed as follows:

$$\sigma_{11}(x_1,0) = -Cp(x_1) + \frac{D}{\pi}\int_{-a}^{b}\frac{p\,(t_1)}{t_1 - x_1}\mathrm{d}t_1 - \frac{\delta^{3/2}}{\pi\lambda_2}\int_{-a}^{b}J_{21}\,(t_1,x_1)p\,(t_1)\,\mathrm{d}t_1 - \frac{\eta\delta^{1/2}}{\pi\lambda_2}\int_{-a}^{b}J_{22}\,(t_1,x_1)\,p\,(t_1)\mathrm{d}t_1, \tag{48}$$

where

$$C = \left(\frac{\omega_2}{\lambda_2} + \nu\right)\delta^2, \quad D = \frac{\eta\delta}{\lambda_2}. \tag{49a,b}$$

In nondimensional form, the in-plane stress component can be expressed as

$$\sigma_{11}(r,0) = -Cp(r) + \frac{D}{\pi}\int_{-1}^{1}\frac{p(s)}{s-r}\mathrm{d}s - \frac{\delta}{\pi\lambda_2}\int_{-1}^{1}\left[\delta J_{21}^{*}(s,r) + \eta J_{22}^{*}(s,r)\right]p(s)\mathrm{d}s. \tag{50}$$

6 Examples

6.1 Flat stamp

Consider the frictional sliding contact problem for the orthotropic half-plane shown in Fig. 3a where the stamp profile is given by

$$u_2(x_1,0) = v_0 = \text{constant}, \quad \frac{\partial}{\partial x_1}u_2(x_1,0) = 0. \tag{51}$$

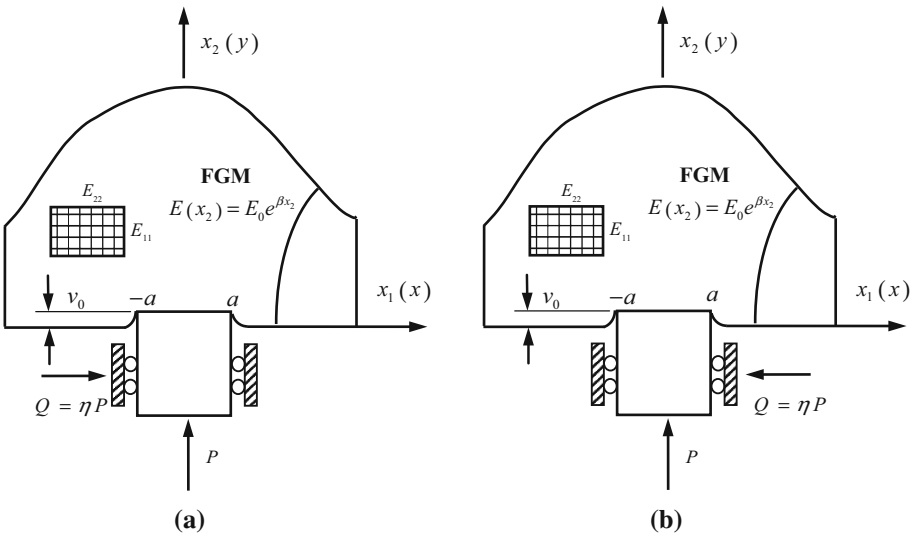

Fig. 3 Flat stamp in sliding frictional contact with graded orthotropic half-plane. **a** $\eta > 0$, **b** $\eta < 0$

Referring to Fig. 3a, and (37), the integral equation (31) and the equilibrium equation (25) become

$$A\phi(r) + \frac{\delta}{\pi}\int_{-1}^{1}\frac{\phi(s)}{s-r}\mathrm{d}s - \frac{1}{\pi}\int_{-1}^{1}\left[\delta J_{11}^{*}(s,r) + \eta J_{12}^{*}(s,r)\right]\phi(s)\mathrm{d}s = 0, \quad -1 < r < 1, \tag{52}$$

$$\int_{-1}^{1}\phi(s)\mathrm{d}s = \frac{P}{\lambda_1 a}. \tag{53}$$

The function $p(x)$ has integrable singularities at $x_1 = a$ and $x_1 = -a$. Thus, from the physics of the problem, we must require that both α and β in the weight function of $\phi(s)$ [see Eq. (35)] be negative. They may then be obtained by letting $N_0 = -1$ and $M_0 = 0$ in Eq. (36) as follows:

$$\begin{aligned}
&\eta > 0: \quad \alpha = -\frac{\theta}{\pi}, \quad \beta = \frac{\theta}{\pi} - 1,\\
&\eta = 0: \quad \alpha = -0.5, \quad \beta = -0.5,\\
&\eta < 0: \quad \alpha = \frac{\theta}{\pi} - 1, \quad \beta = -\frac{\theta}{\pi},
\end{aligned} \tag{54}$$

with

$$\theta = \arctan\left|\frac{\delta}{\eta\omega_1}\right|, \quad 0 < \theta < \frac{\pi}{2}, \tag{55}$$

where ω_1 is given in Appendix C. Assuming a solution of the form (37), using the properties of Jacobi polynomials, and truncating the series at N, Eq. (40) becomes

$$\sum_{0}^{N} c_n\left[-\frac{\delta}{2\sin(\pi\alpha)}P_{n-1}^{(-\alpha,-\beta)}(r) + h_n^1(r) + h_n^2(r)\right] = 0. \tag{56}$$

Using the collocation technique, (56) gives N equations for $N+1$ unknown constants $c_0, \ldots, c_N$. The additional equation for a unique solution is provided by the equilibrium condition (53), which becomes

$$\sum_{n=0}^{N} c_n^{*}\int_{-1}^{1} w(s)P_n^{(\alpha,\beta)}(s)\mathrm{d}s = 1, \tag{57}$$

where

$$c_n^{*} = \frac{\lambda_1 a}{P}c_n. \tag{58}$$

Using the following orthogonality condition

$$\int_{-1}^{1} P_n^{(\alpha,\beta)}(t)P_j^{(\alpha,\beta)}(t)w(t)\mathrm{d}t = \begin{cases} 0 & n \neq j,\\ \theta_j^{(\alpha,\beta)} & n = j, \end{cases} \tag{59}$$

where

$$\theta_0(\alpha,\beta) = \int_{-1}^{1} w(t)\mathrm{d}t = \frac{2^{\alpha+\beta+1}\Gamma(\alpha+1)\Gamma(\beta+1)}{\Gamma(\alpha+\beta+2)}, \tag{60}$$

$$\theta_j(\alpha,\beta) = \frac{2^{\alpha+\beta+1}\Gamma(j+\alpha+1)\Gamma(j+\beta+1)}{(2j+\alpha+\beta+1)j!\Gamma(j+\alpha+\beta+1)}, \tag{61}$$

we obtain the following $N+1$ equations

$$c_0^{*}\theta_0 = 1, \quad \sum_{n=1}^{N} c_n^{*}F_n(r_i) = 0, \quad i = 1, \ldots, N, \tag{62a,b}$$

where

$$F_n(r_i) = -\frac{\delta}{2\sin(\pi\alpha)} P_{n-1}^{(-\alpha,-\beta)}(r_i) + h_n^1(r_i) + h_n^2(r_i). \tag{63}$$

In (63), r_i $(i = 1, \ldots, N)$ are obtained by letting

$$P_{N-1}^{(\alpha+1,\beta+1)}(r_i) = 0, \quad i = 1, \ldots, N. \tag{64}$$

After determining c_n, the contact stresses and the in-plane stress may be obtained as

$$\frac{\sigma_{22}(x_1,0)}{\sigma_0} = -\frac{p(x_1)}{\sigma_0}, \tag{65a}$$

$$\frac{\sigma_{12}(x_1,0)}{\sigma_0} = -\eta\frac{p(x_1)}{\sigma_0}, \tag{65b}$$

$$\frac{\sigma_{11}(r,0)}{\sigma_0} = -\frac{C}{\sigma_0}p(r) + \frac{D}{\pi\sigma_0}\int_{-1}^{1}\frac{p(s)}{s-r}\mathrm{d}s - \frac{\delta}{\pi\lambda_2\sigma_0}\int_{-1}^{1}\left[\delta J_{21}^*(s,r) + \eta J_{22}^*(s,r)\right]p(s)\mathrm{d}s, \tag{65c}$$

$$\sigma_0 = \frac{P}{2a}, \tag{65d}$$

where

$$p(x_1) = 2\sigma_0\left(1-\frac{x_1}{a}\right)^{\alpha}\left(1+\frac{x_1}{a}\right)^{\beta}\sum_{n=0}^{N} c_n^* P_n^{(\alpha,\beta)}\left(\frac{x_1}{a}\right), \quad -a < x_1 < a. \tag{66}$$

Upon solving the problem, the stress intensity factors at the end points $x_1 = \pm a$ of the flat stamp may be defined as and evaluated from

$$k_p(a) = \lim_{x_1\to a}\frac{p(x_1)}{2^{\beta}(a-x_1)^{\alpha}} = Pa^{\beta}\sum_{n=0}^{N} c_n^* P_n^{(\alpha,\beta)}(1), \tag{67a}$$

$$k_p(-a) = \lim_{x_1\to -a}\frac{p(x_1)}{2^{\alpha}(x_1+a)^{\beta}} = Pa^{\alpha}\sum_{n=0}^{N} c_n^* P_n^{(\alpha,\beta)}(-1), \tag{67b}$$

or in nondimensional form:

$$k_p^*(a) = \frac{k_p(a)}{Pa^{\beta}} = \sum_{n=0}^{N} c_n^* P_n^{(\alpha,\beta)}(1), \tag{68a}$$

$$k_p^*(-a) = \frac{k_p(-a)}{Pa^{\alpha}} = \sum_{n=0}^{N} c_n^* P_n^{(\alpha,\beta)}(-1). \tag{68b}$$

6.2 Wedge stamp

Consider the frictional sliding contact problem for the graded orthotropic half-plane indented by a wedge stamp shown in Fig. 4a where the stamp profile is given by

$$u_2(x_1,0) = -mx_1 + \mathrm{C}, \quad \frac{\mathrm{d}}{\mathrm{d}x_1}u_2(x_1,0) = -m, \tag{69}$$

where m is a positive constant. The following definitions are used in normalizing the integral equation:

$$x = \frac{b}{2\sqrt{\delta}}(r+1), \quad t = \frac{b}{2\sqrt{\delta}}(s+1), \quad p(s) = \lambda_1 E_0^* \phi(s), \tag{70}$$

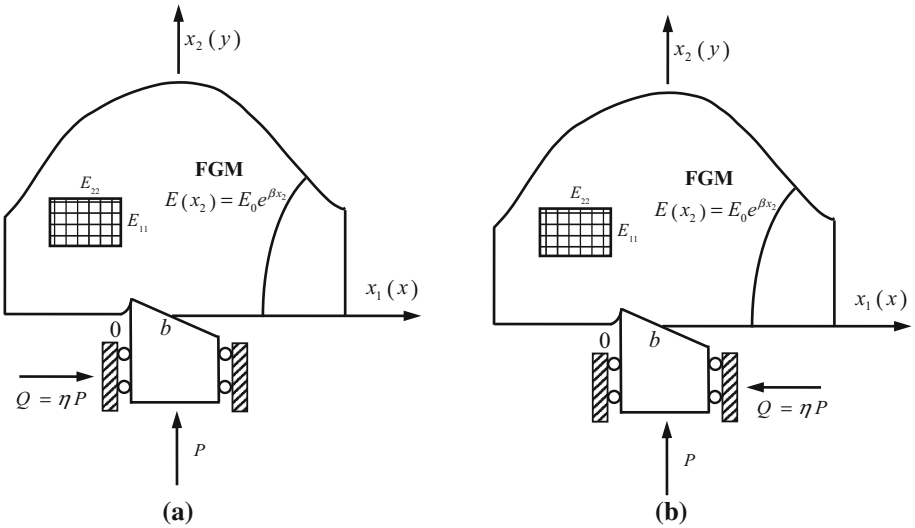

Fig. 4 Wedge stamp in sliding frictional contact with graded orthotropic half-plane. **a** $\eta > 0$, **b** $\eta < 0$

where E_0^* is given in Eq. (9c). Referring to Fig. 4a, the integral equation (31) and the equilibrium equation (25) become

$$A\phi(r) + \frac{B}{\pi}\int_{-1}^{1}\frac{\phi(s)}{s-r}\mathrm{d}s - \frac{\delta}{\pi}\int_{-1}^{1}J_{11}^{*}(s,r)\phi(s)\mathrm{d}s - \frac{\eta}{\pi}\int_{-1}^{1}J_{12}^{*}(s,r)\phi(s)\mathrm{d}s = -m, \tag{71}$$

$$\int_{-1}^{1}\phi(s)\mathrm{d}s = \frac{2P}{\lambda_1 E_0^* b}. \tag{72}$$

Since the wedge stamp has a sharp corner at $x_1 = 0$ and a smooth contact at $x_1 = b$ from the physics of the problem, it is obvious that α must be positive and β must be negative in the weight function of $\phi(s)$. They can be found by letting $M_0 = N_0 = 0$ in Eq. (36) as

$$\begin{aligned}
&\eta > 0: \quad \alpha = 1 - \frac{\theta}{\pi}, \quad \beta = -1 + \frac{\theta}{\pi},\\
&\eta = 0: \quad \alpha = 0.5, \quad \beta = -0.5,\\
&\eta < 0: \quad \alpha = \frac{\theta}{\pi}, \quad \beta = -\frac{\theta}{\pi},
\end{aligned} \tag{73}$$

where θ is given by Eq. (55). Assuming a solution of the form (37) and using the properties of Jacobi polynomials, and truncating the series at N, Eq. (40) becomes

$$\sum_{0}^{N} c_n^{*}\left[-\frac{\delta}{\sin(\pi\alpha)}P_n^{(-\alpha,-\beta)}(r) + h_n^1(r) + h_n^2(r)\right] = -1, \quad -1 < r < 1, \tag{74a}$$

$$c_n^{*} = \frac{c_n}{m}. \tag{74b}$$

In this problem, after the application of the load P, one end of the contact length, namely b, is unknown. However, for a given value of the contact length, Eq. (74) provides $N+1$ equations for $N+1$ unknown constants $(c_0^{*}, \ldots, c_N^{*})$ as follows:

$$\begin{aligned}
&\sum_{0}^{N} c_n^{*}\left[-\frac{\delta}{\sin(\pi\alpha)}P_n^{(-\alpha,-\beta)}(r_i) + h_n^1(r_i) + h_n^2(r_i)\right] = -1,\\
&i = 1, \ldots, N+1, \quad -1 < r < 1,
\end{aligned} \tag{75}$$

where $(r_i, i = 0, 1, \ldots, N+1)$ are defined by

$$P_{N+1}^{(\alpha-1,\beta+1)}(r_i)=0 \quad (r_i,\ i=0,1,\ldots,N+1)\,. \tag{76}$$

The relationship between the applied load P and the contact length b can be found from the equilibrium equation (72) as:

$$c_0^*\theta_0=\frac{2P}{\lambda_1 E_0^* m b}, \tag{77}$$

where θ_0 can be computed from Eq. (55) as

$$\theta_0=\frac{2\pi\alpha}{\sin\pi\alpha}. \tag{78}$$

The relation between the applied load P and the contact length b then becomes

$$\frac{P}{E_0^* m}=\frac{c_0^*\theta_0\lambda_1}{2}b. \tag{79}$$

The contact stresses in nondimensional form at the surface of the graded orthotropic half-plane can then be expressed as

$$\frac{\sigma_{22}(x_1,0)}{E_0^* m}=-\frac{p(x_1)}{E_0^* m}, \tag{80a}$$

$$\frac{\sigma_{12}(x_1,0)}{E_0^* m}=-\eta\frac{p(x_1)}{E_0^* m}, \tag{80b}$$

$$\frac{\sigma_{11}(r,0)}{E_0^* m}=-\frac{C}{E_0^* m}p(r)+\frac{D}{\pi E_0^* m}\int_{-1}^{1}\frac{p(s)}{s-r}\mathrm{d}s-\frac{\delta}{\pi\lambda_2 E_0^* m}\int_{-1}^{1}\left[\delta J_{21}^*(s,r)+\eta J_{22}^*(s,r)\right]p(s)\mathrm{d}s, \tag{80c}$$

where

$$p(x_1)=E_0^* m\lambda_1\left(\frac{b-x_1}{x_1}\right)^{\alpha}\sum_{n=0}^{N}c_n^* P_n^{(\alpha,\beta)}\left(\frac{2x_1}{b}-1\right). \tag{81}$$

After determining c_n^*, the stress intensity factor at $x_1=0$ may be defined as

$$k_p(0)=\lim_{x_1\to 0}(x_1)^{\alpha}p(x_1)=\lambda_1 m E_0^* b^{\alpha}\sum_{n=0}^{N}c_n^* P_n^{(\alpha,\beta)}(-1), \tag{82}$$

or in nondimensional form

$$k_p^*(0)=\frac{k_p(0)}{m E_0^* b^{\alpha}}=\lambda_1\sum_{n=0}^{N}c_n^* P_n^{(\alpha,\beta)}(-1). \tag{83}$$

7 Results and discussion

This section introduces the numerical results of the problem described in Figs. 3 and 4 where the graded orthotropic half-plane is loaded by a sliding rigid flat and wedge stamp, respectively. Note that, depending on the direction of the lateral force Q, the friction coefficient is taken to be positive (Figs. 3a, 4a) or negative (Figs. 3b, 4b) in the remaining figures. The material properties of the orthotropic medium are defined with four effective elastic parameters, namely the effective stiffness, E, the effective Poisson' s ratio, ν, the stiffness ratio, δ, and the shear parameter, κ, given in Eqs. (1–2).

As described in the paper by Ozturk and Erdogan [65,66], the physically acceptable solution is only available when the elastic parameters have the following range ($-1<\kappa<\infty$, $0<\nu<1$, $\kappa+\nu>0$). Therefore, in this study, the results are obtained for the following range of elastic parameters ($-0.1\le\kappa\le 5.0$, $0.2\le\delta^4\le 5.0$, $1/7\le\nu\le 5/7$, $-0.9\le\eta\le 0.9$, $0.0\le\beta a\le 3.0$, $0.0\le\beta b\le 6.0$,). In all of the results given herein, the plane strain assumption is used.

Table 1 shows the comparison of homogeneous and graded orthotropic elastic parameters appearing in Eqs. (21) and (23) for the nonhomogeneity parameter, $\beta a=0.001$. In the limiting case, as the coefficient of

friction, $\eta \to 0$, approaches zero, $\theta \to \pi/2$, $\alpha \to -1/2$, and $\beta \to -1/2$ (see Eq. 36 or 54), we recover the known square-root singularity for the frictionless sliding flat stamp (see the results in Tables 2, 3). Note that as the stiffness ratio, δ, tends to 1 from the right or left, isotropic results are recovered as shown in Table 2. Similarly as the shear parameter, κ, tends to 1 from right or left, we recover the isotropic results given in Table 3 for ($\kappa = 1$ and $\delta^4 = 1$).

Tables 4 and 5 list the strength of stress singularity α and β, respectively, for a flat stamp. As the magnitude of the coefficient of friction increases, the strength of stress singularity at the trailing edge, α, increases for $\eta < 0$. And as η becomes very large, $\theta \to 0$, $\alpha \to -1$, and $\beta \to 0$. However, for $\eta > 0$, as the magnitude of the coefficient of friction increases, the strength of stress singularity at the trailing edge, β, increases and as η becomes very large, $\theta \to 0$, $\beta \to -1$, and $\alpha \to 0$ (see Table 5). Note that Tables 4 and 5 for $\eta < 0$ are exactly the same as Tables 2 and 3 of Ref. [57].

Table 6 displays the stress intensity factor results for an orthotropic inhomogeneous medium loaded by a flat stamp as shown in Fig. 3b ($\eta < 0$) for various values of the inhomogeneity parameter βa. Observe that when $\beta a \to 0$, we recover the homogeneous orthotropic results given by Ref. [57].

Stress intensity factors for various values of the coefficient of friction and inhomogeneity parameter are given in Tables 7, 8, and 9 for fixed values of the shear parameter and the effective Poisson's ratio while varying the stiffness parameter at $\delta^4 = 0.5, 2, 8$, respectively. As the stiffness parameter increases, the stress intensity factors increase. And in general, as the inhomogeneity parameter increases, the stress intensity factors decrease.

Table 1 Comparison of homogeneous and graded orthotropic elastic parameters appearing in Eqs. (21) and (23) for $\nu = 3/7$

κ	ω_1	ω_1^{ort}	ω_2	ω_2^{ort}	λ_1	λ_1^{ort}	λ_2	λ_2^{ort}
−0.25	0.4666	0.4670	0.4666	0.4661	0.8165	0.8163	0.8165	0.8160
0	0.4040	0.4044	0.4040	0.4043	0.7070	0.7067	0.7070	0.7065
0.5	0.3300	0.3302	0.3300	0.3297	0.5775	0.5775	0.5775	0.5775
1.0	0.2857	0.2857	0.2857	0.2857	0.5000	0.5000	0.5000	0.5000
2.0	0.2332	0.2338	0.2332	0.2330	0.4082	0.4076	0.4082	0.4080
5.0	0.1650	0.1629	0.1650	0.1682	0.2887	0.2916	0.2887	0.2882

Table 2 Stress intensity factors at the sharp edges of the flat stamp with the parameters $\kappa = 0.99$, $\nu = 3/7$, $\eta = 0.0$, $\alpha = -0.5$, $\beta = -0.5$

βa	$\frac{k_p(-a)}{Pa^\alpha} = \frac{k_p(a)}{Pa^\beta}$				
	$\delta^4 = 0.9$	$\delta^4 = 0.99$	$\delta^4 = 1.0$	$\delta^4 = 1.01$	$\delta^4 = 1.1$
0.0	0.3183	0.3183	0. 3183	0.3183	0.3183
0.01	0.3159	0.3159	0.3159	0.3159	0.3160
0.1	0.2972	0.2976	0.2976	0.2977	0.2981
0.4	0.2543	0.2554	0.2554	0.2556	0.2565
0.7	0.2258	0.2272	0.2272	0.2274	0.2286
1.0	0.2049	0.2063	0.2064	0.2066	0.2079
2.0	0.1617	0.1632	0.1633	0.1635	0.1649

Table 3 Stress intensity factors at the sharp edges of the flat stamp with the parameters, $\delta^4 = 1.0$, $\nu = 3/7$, $\eta = 0.0$, $\alpha = -0.5$, $\beta = -0.5$

βa	$\frac{k_p(-a)}{Pa^\alpha} = \frac{k_p(a)}{Pa^\beta}$				
	$\kappa = 0.9$	$\kappa = 0.99$	$\kappa = 1.0$	$\kappa = 1.01$	$\kappa = 1.1$
0.0	0.3183	0.3183	0. 3183	0.3183	0.3183
0.01	0.3160	0.3159	0.3159	0.3159	0.3159
0.1	0.2979	0.2977	0.2976	0.2976	0.2973
0.4	0.2562	0.2555	0.2554	0.2448	0.2440
0.7	0.2282	0.2273	0.2272	0.2063	0.2053
1.0	0.2075	0.2065	0.2064	0.1631	0.1621
2.0	0.1645	0.1634	0.1633	0.1387	0.1377

The effect of the shear parameter on the stress intensity factors for the flat stamp can be seen by comparing Tables 7 and 10 for $\kappa = 0.5$ vs. $\kappa = 2.0$, respectively. As the shear parameter increases, the stress intensity factors decrease at both ends of the flat stamp.

Table 11 demonstrates the stress intensity factor results for an orthotropic inhomogeneous medium loaded by a wedge stamp as shown in Fig. 4b for various values of the inhomogeneity parameter βb. Observe that when we recover the homogeneous orthotropic results given by Ref. [58].

The effect of the inhomogeneity on the stress intensity factor for the wedge stamp for various values of the shear parameter for the frictionless and frictional contact cases is shown in Table 12. As the shear parameter κ gets larger, the stress intensity factor decreases in all cases. The same table in terms of the variation of the stiffness ratio, δ, is presented in Table 13. As the stiffness ratio δ gets larger, the stress intensity factor decreases in all cases.

Figures 5, 6, 7, 8, 9, and 10 illustrate contact pressure distribution obtained for a flat stamp configuration as shown in Fig. 3a or b depending on the direction of the lateral force Q. The contact pressure is normalized with $\sigma_0 = \frac{P}{2a}$. The numerical results of this study are first validated by the results obtained by Ref. [67] where the same problem is considered for a graded isotropic graded half-plane. In order to capture the isotropic behavior from an orthotropic formulation, the material elastic parameters are set at $\kappa = 0.99$ and $\delta^4 = 1$. An excellent match is obtained for the flat stamp as depicted in Fig. 5a, b for the coefficient of friction $\eta = 0$ and $\eta = 0.5$, respectively. The next validation is done with Ref. [57] where the same problem is considered for a homogeneous orthotropic half-plane (see the red dots in Fig. 6 for the inhomogeneity parameter $\beta a = 0$). Again an excellent match is observed. Figure 6 demonstrates how the material property grading affects the contact pressure distribution. As the inhomogeneity parameter increases, the curves at the center of the contact becomes more flatter for frictionless contact ($\eta = 0$) where the strength of power singularities $\alpha = \beta = -1/2$. For the frictional contact where $\eta \neq 0$, the distribution is not symmetric. Depending on the shear parameter, the contact pressure slants toward either to the leading or to the trailing edge of the contact. Similarly, Fig. 7 depicts the contact pressure results when the direction of the lateral force Q is changed.

Contact pressure distribution for various values of the stiffness ratio, $\delta^4 = \frac{E_{11}}{E_{22}}$, is plotted in the range $0.2 \leq \delta^4 \leq 5.0$ for different values of the shear parameter, κ, and the coefficient of friction ($\eta > 0$) as shown in the insert in Fig. 7. As the coefficient of friction increases, the curves slant toward the leading edge when the shear parameter κ is less than one and to the trailing edge when the shear parameter is greater than one. Observe that as the stiffness ratio δ increases, the contact pressure distribution becomes more symmetric even for the frictional contact (see Fig. 7).

In Fig. 8a, b, contact pressure is plotted for a graded orthotropic half-plane where the inhomogeneity parameter $\beta a = 1$ and the friction coefficient is $\eta = 0.5$ for various values of the shear parameter κ. Note that as the shear parameter κ increases, the stress distribution is slanted toward the trailing edge for $\delta^4 = 0.25$. As the shear parameter gets smaller, the stress distribution is slanted toward the leading edge. The effect of the effective Poisson's ratio ν, on the contact pressure distribution, can be seen in Fig. 8c, d. The direction of slant in these curves moves from the leading edge to the trailing edge as ν increases when stiffness ratio $\delta^4 = 0.25$ for the graded orthotropic half-plane with an inhomogeneity parameter $\beta a = 1$. The same set of figures is drawn for $\delta^4 = 2$ in Fig. 8d for comparison. Note that the contact pressure in the middle of the stamp is higher for $\delta^4 = 2$ as compared to $\delta^4 = 0.25$.

Figure 9 shows the effect of the coefficient of friction on the contact pressure distribution for various values of the shear parameter and the stiffness ratio. Note that there is not a significant change in the contact pressure as the shear parameter gets larger for higher values of the stiffness ratio (see Fig. 9f). The curves slant toward the leading edge for small shear parameter and to the trailing edge as the shear parameter gets larger.

As mentioned in Sect. 5, the in-plane component of the stress component $\sigma_{11}(x_1, 0)$ may lead to the surface damage or crack initiation when it becomes tensile at the surface. Figures 10 and 11 depict the distribution of this stress component in the case of negative and positive values of the coefficient of friction for orthotropic homogeneous materials. Note that when $\eta < 0$, the direction of the lateral component of the applied force to the stamp is toward right, and when $\eta > 0$, it is toward left. In Fig. 10, the in-plane stress is tensile at the trailing region ($r > 1$, or $x_1 > a$) for $\eta < 0$. Observe that the in-plane stress is tensile at $r < 1$, or $x_1 < -a$ when the direction of the lateral force, Q, is changed ($\eta > 0$).

The stress results for a wedge stamp are also validated by the results obtained by Guler [67] as depicted in Fig. 12a, b by setting the elastic parameters $\delta^4 = 1$ and the shear parameter is almost equal to 1 ($\kappa = 0.99$). To make these validations, contact stresses are normalized with P/b, the same convention used in [67]:

Table 4 Strength of stress singularity α for the flat stamp $\nu = 3/7$

	α											
	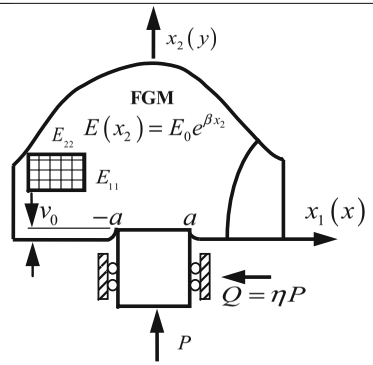						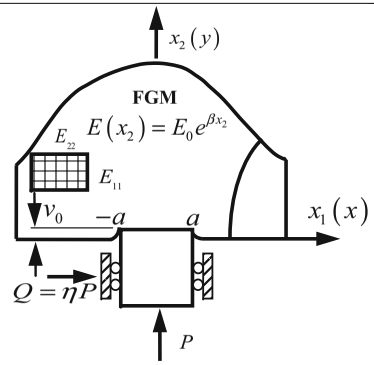					
δ^4	$\eta = -0.9$			$\eta = -0.5$			$\eta = 0.5$			$\eta = 0.9$		
	$\kappa = -0.1$	$\kappa = 0.99$	$\kappa = 5$	$\kappa = -0.1$	$\kappa = 0.99$	$\kappa = 5$	$\kappa = -0.1$	$\kappa = 0.99$	$\kappa = 5$	$\kappa = -0.1$	$\kappa = 0.99$	$\kappa = 5$
0.2	−0.6657	−0.6171	−0.5695	−0.5981	−0.5672	−0.5391	−0.4019	−0.4328	−0.4609	−0.3343	−0.3829	−0.4305
1.0	−0.6165	−0.5803	−0.5469	−0.5668	−0.5453	−0.5262	−0.4332	−0.4547	−0.4738	−0.3835	−0.4197	−0.4531
5.0	−0.5799	−0.5543	−0.5315	−0.5450	−0.5304	−0.5175	−0.4550	−0.4696	−0.4825	−0.4201	−0.4457	−0.4685

Table 5 Strength of stress singularity β for the flat stamp $\nu = 3/7$

	β											
	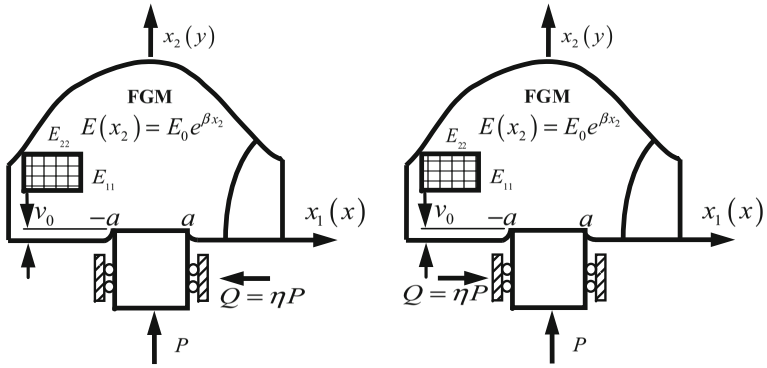										
δ^4	$\eta = -0.9$			$\eta = -0.5$			$\eta = 0.5$			$\eta = 0.9$		
	$\kappa = -0.1$	$\kappa = 0.99$	$\kappa = 5$	$\kappa = -0.1$	$\kappa = 0.99$	$\kappa = 5$	$\kappa = -0.1$	$\kappa = 0.99$	$\kappa = 5$	$\kappa = -0.1$	$\kappa = 0.99$	$\kappa = 5$
0.2	−0.3343	−0.3829	−0.4305	−0.4019	−0.4328	−0.4609	−0.5981	−0.5672	−0.5391	−0.6657	−0.6171	−0.5695
1.0	−0.3835	−0.4197	−0.4531	−0.4332	−0.4547	−0.4738	−0.5668	−0.5453	−0.5262	−0.6165	−0.5803	−0.5469
5.0	−0.4201	−0.4457	−0.4685	−0.4550	−0.4696	−0.4825	−0.5450	−0.5304	−0.5175	−0.5799	−0.5543	−0.5315

Table 6 Stress intensity factors at the sharp edges of the flat stamp (see Fig. 3b) with the parameters, $\delta^4 = 0.2$, $\eta = -0.5$, $\nu = 3/7$

βa	$\kappa = -0.1$		$\kappa = 0.99$		$\kappa = 5.0$	
	$\alpha = -0.5981$		$\alpha = -0.5672$		$\alpha = -0.5391$	
	$\beta = -0.4019$		$\beta = -0.4328$		$\beta = -0.4609$	
	$\frac{k_p(-a)}{Pa^\alpha}$	$\frac{k_p(a)}{Pa^\beta}$	$\frac{k_p(-a)}{Pa^\alpha}$	$\frac{k_p(a)}{Pa^\beta}$	$\frac{k_p(-a)}{Pa^\alpha}$	$\frac{k_p(a)}{Pa^\beta}$
0.0*	0.3033	0.3033	0.3113	0.3113	0.3159	0.3159
0.01	0.3069	0.2962	0.3140	0.3030	0.3162	0.3058
0.1	0.3055	0.2628	0.3077	0.2629	0.2965	0.2551
0.4	0.2782	0.2074	0.2725	0.1974	0.2469	0.1761
0.7	0.2556	0.1765	0.2460	0.1625	0.2191	0.1375
1.0	0.2381	0.1554	0.2262	0.1400	0.2009	0.1142
2.0	0.2002	0.1155	0.1845	0.1005	0.1668	0.0767

* Reference [57]

Table 7 Stress intensity factors at the sharp edges of the flat stamp (see Fig. 3a) with the parameters, $\kappa = 0.5$, $\delta^4 = 0.5$, $\nu = 3/7$

βa	$\eta = 0.0$		$\eta = 0.1$		$\eta = 0.3$		$\eta = 0.5$	
	$\alpha = -0.5000$		$\alpha = -0.4875$		$\alpha = -0.4627$		$\alpha = -0.4383$	
	$\beta = -0.5000$		$\beta = -0.5125$		$\beta = -0.5373$		$\beta = -0.5617$	
	$\frac{k_p(-a)}{Pa^\alpha} = \frac{k_p(a)}{Pa^\beta}$		$\frac{k_p(-a)}{Pa^\alpha}$	$\frac{k_p(a)}{Pa^\beta}$	$\frac{k_p(-a)}{Pa^\alpha}$	$\frac{k_p(a)}{Pa^\beta}$	$\frac{k_p(-a)}{Pa^\alpha}$	$\frac{k_p(a)}{Pa^\beta}$
0.0	0.3183		0.3181	0.3181	0.3161	0.3161	0.3123	0.3124
0.01	0.3157		0.3147	0.3163	0.3114	0.3160	0.3065	0.3140
0.1	0.2961		0.2927	0.2992	0.2849	0.3045	0.2762	0.3084
0.4	0.2520		0.2462	0.2577	0.2342	0.2686	0.2220	0.2784
0.7	0.2232		0.2166	0.2298	0.2034	0.2425	0.1903	0.2545
1.0	0.2023		0.1953	0.2091	0.1817	0.2227	0.1684	0.2358
2.0	0.1595		0.1525	0.1665	0.1391	0.1806	0.1264	0.1946

Table 8 Stress intensity factors at the sharp edges of the flat stamp (see Fig. 3a) with the parameters, $\kappa = 0.5$, $\delta^4 = 2.0$, $\nu = 3/7$

βa	$\eta = 0.0$		$\eta = 0.1$		$\eta = 0.3$		$\eta = 0.5$	
	$\alpha = -0.5000$		$\alpha = -0.4912$		$\alpha = -0.4736$		$\alpha = -0.4561$	
	$\beta = -0.5000$		$\beta = -0.5088$		$\beta = -0.5264$		$\beta = -0.5439$	
	$\frac{k_p(-a)}{Pa^\alpha} = \frac{k_p(a)}{Pa^\beta}$		$\frac{k_p(-a)}{Pa^\alpha}$	$\frac{k_p(a)}{Pa^\beta}$	$\frac{k_p(-a)}{Pa^\alpha}$	$\frac{k_p(a)}{Pa^\beta}$	$\frac{k_p(-a)}{Pa^\alpha}$	$\frac{k_p(a)}{Pa^\beta}$
0.0	0.3183		0.3182	0.3182	0.3172	0.3172	0.3153	0.3153
0.01	0.3165		0.3159	0.3168	0.3142	0.3167	0.3116	0.3157
0.1	0.3019		0.2999	0.3038	0.2954	0.3069	0.2903	0.3094
0.4	0.2667		0.2630	0.2703	0.2553	0.2772	0.2474	0.2835
0.7	0.2418		0.2374	0.2461	0.2286	0.2544	0.2197	0.2624
1.0	0.2226		0.2180	0.2273	0.2086	0.2364	0.1992	0.2453
2.0	0.1809		0.1759	0.1859	0.1661	0.1958	0.1565	0.2060

Table 9 Stress intensity factors at the sharp edges of the flat stamp (see Fig. 3a) with the parameters, $\kappa = 0.5$, $\delta^4 = 8.0$, $\nu = 3/7$

βa	$\eta = 0.0$		$\eta = 0.1$		$\eta = 0.3$		$\eta = 0.5$	
	$\alpha = -0.5000$		$\alpha = -0.4938$		$\alpha = -0.4813$		$\alpha = -0.4689$	
	$\beta = -0.5000$		$\beta = -0.5062$		$\beta = -0.5187$		$\beta = -0.5311$	
	$\frac{k_p(-a)}{Pa^\alpha} = \frac{k_p(a)}{Pa^\beta}$		$\frac{k_p(-a)}{Pa^\alpha}$	$\frac{k_p(a)}{Pa^\beta}$	$\frac{k_p(-a)}{Pa^\alpha}$	$\frac{k_p(a)}{Pa^\beta}$	$\frac{k_p(-a)}{Pa^\alpha}$	$\frac{k_p(a)}{Pa^\beta}$
0.0	0.3183		0.3182	0.3182	0.3178	0.3178	0.3168	0.3168
0.01	0.3170		0.3167	0.3172	0.3158	0.3172	0.3144	0.3167
0.1	0.3064		0.3052	0.3074	0.3026	0.3093	0.2996	0.3108
0.4	0.2788		0.2765	0.2810	0.2717	0.2853	0.2668	0.2893
0.7	0.2580		0.2552	0.2607	0.2495	0.2661	0.2437	0.2713
1.0	0.2412		0.2382	0.2443	0.2319	0.2503	0.2257	0.2561
2.0	0.2023		0.1988	0.2057	0.1919	0.2126	0.1851	0.2194

Table 10 Stress intensity factors at the sharp edges of the flat stamp (see Fig. 3a) with the parameters, $\kappa = 2.0,\ \delta^4 = 0.5, \nu = 3/7$

βa	$\eta = 0.0$		$\eta = 0.1$		$\eta = 0.3$		$\eta = 0.5$	
	$\alpha = -0.5000$		$\alpha = -0.4912$		$\alpha = -0.4736$		$\alpha = -0.4561$	
	$\beta = -0.5000$		$\beta = -0.5088$		$\beta = -0.5264$		$\beta = -0.5439$	
	$\frac{k_p(-a)}{Pa^\alpha} = \frac{k_p(a)}{Pa^\beta}$		$\frac{k_p(-a)}{Pa^\alpha}$	$\frac{k_p(a)}{Pa^\beta}$	$\frac{k_p(-a)}{Pa^\alpha}$	$\frac{k_p(a)}{Pa^\beta}$	$\frac{k_p(-a)}{Pa^\alpha}$	$\frac{k_p(a)}{Pa^\beta}$
0.0	0.3183		0.3182	0.3182	0.3172	0.3172	0.3153	0.3153
0.01	0.3151		0.3142	0.3157	0.3118	0.3163	0.3087	0.3161
0.1	0.2910		0.2878	0.2941	0.2809	0.3000	0.2736	0.3052
0.4	0.2396		0.2339	0.2453	0.2227	0.2565	0.2115	0.2675
0.7	0.2079		0.2015	0.2145	0.1888	0.2277	0.1765	0.2409
1.0	0.1858		0.1790	0.1927	0.1658	0.2069	0.1532	0.2213
2.0	0.1429		0.1360	0.1500	0.1229	0.1650	0.1108	0.1807

Table 11 Stress intensity factors for the wedge stamp (see Fig. 4b) with the parameters $\delta^4 = 0.2, \eta = -0.5, \nu = 3/7$

βb	$\kappa = -0.1$ $\alpha = 0.4019$ $\beta = -0.4019$	$\kappa = 0.99$ $\alpha = 0.4328$ $\beta = -0.4328$	$\kappa = 5.0$ $\alpha = 0.4609$ $\beta = -0.4609$
	$\frac{k_p(0)}{mE_0^* b^\alpha}$	$\frac{k_p(0)}{mE_0^* b^\alpha}$	$\frac{k_p(0)}{mE_0^* b^\alpha}$
0.0*	1.0621	0.7330	0.4285
0.2	1.2267	0.8684	0.5312
1.0	1.6528	1.2461	0.8474
2.0.	2.0854	1.6416	1.1989
4.0	2.8231	2.3049	1.8051

* Reference [58]

Table 12 Stress intensity factors for the wedge stamp (see Fig. 4a) with the parameters, $\delta^4 = 2.0, \nu = 3/7$

βb	$\eta = 0.0$			$\eta = 0.9$		
	$\kappa = -0.25$ $\alpha = 0.5000$ $\beta = -0.5000$	$\kappa = 0.5$ $\alpha = 0.5000$ $\beta = -0.5000$	$\kappa = 2.0$ $\alpha = 0.5000$ $\beta = -0.5000$	$\kappa = -0.25$ $\alpha = 0.6080$ $\beta = -0.6080$	$\kappa = 0.5$ $\alpha = 0.5779$ $\beta = -0.5779$	$\kappa = 2.0$ $\alpha = 0.5556$ $\beta = -0.5556$
	$\frac{k_p(0)}{mE_0^* b^\alpha}$	$\frac{k_p(0)}{mE_0^* b^\alpha}$	$\frac{k_p(0)}{mE_0^* b^\alpha}$	$\frac{k_p(0)}{mE_0^* b^\alpha}$	$\frac{k_p(0)}{mE_0^* b^\alpha}$	$\frac{k_p(0)}{mE_0^* b^\alpha}$
0.0	0.6866	0.4855	0.3433	0.6474	0.4710	0.3381
0.2	0.7188	0.5120	0.3668	0.6359	0.4664	0.3401
1.0	0.8250	0.6013	0.4456	0.6764	0.5053	0.3802
2.0	0.9356	0.6968	0.5297	0.7334	0.5581	0.4271
4.0	1.1210	0.8611	0.6728	0.8324	0.6527	0.5053

Table 13 Stress intensity factors for the wedge stamp (see Fig. 4a) with the parameters, $\beta b = 1.0,\ \nu = 3/7$

δ^4	$\eta = 0.0$			$\eta = 0.9$		
	$\kappa = -0.25$	$\kappa = 0.5$	$\kappa = 2.0$	$\kappa = -0.25$	$\kappa = 0.5$	$\kappa = 2.0$
	$\frac{k_p(0)}{mE_0^* b^\alpha}$	$\frac{k_p(0)}{mE_0^* b^\alpha}$	$\frac{k_p(0)}{mE_0^* b^\alpha}$	$\frac{k_p(0)}{mE_0^* b^\alpha}$	$\frac{k_p(0)}{mE_0^* b^\alpha}$	$\frac{k_p(0)}{mE_0^* b^\alpha}$
0.25	1.5173	1.1230	0.8478	0.9712	0.7676	0.5978
1.0	1.0076	0.7377	0.5499	0.7755	0.5880	0.4470
3.0	0.7349	0.5343	0.3947	0.6208	0.4606	0.3447
5.0	0.6361	0.4612	0.3394	0.5546	0.4084	0.3037

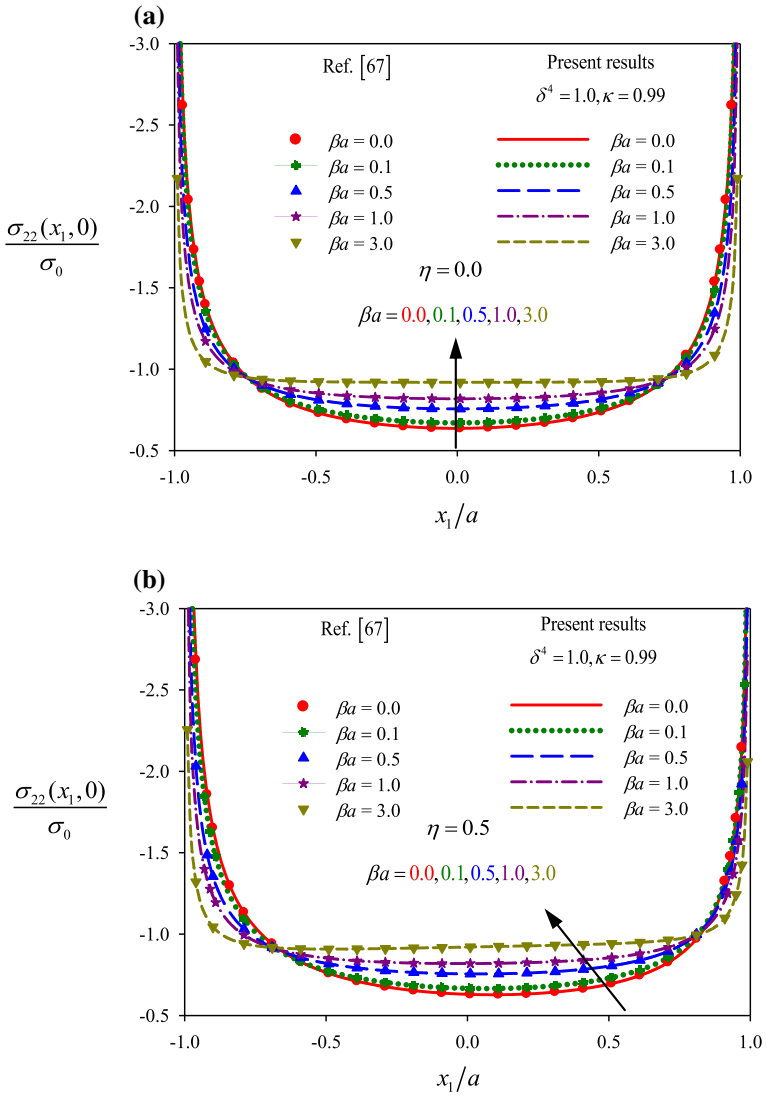

Fig. 5 Contact pressure distribution, $\sigma_{22}(x_1, 0)$, at the surface of graded orthotropic half-plane loaded by a flat stamp for various values of the inhomogeneity parameter, βa, with the parameters $\kappa = 0.99$, $\delta^4 = 1.0$, $\nu = 3/7$, $\sigma_0 = \frac{P}{2a}$, **a** $\eta = 0.0$, **b** $\eta = 0.5$

$$\frac{\sigma_{22}(x_1, 0)}{P/b} = -\frac{2}{c_0\theta_0}\left(\frac{b - x_1}{x_1}\right)^{\alpha} \sum_{n=0}^{N} c_n P_n^{(\alpha,\beta)}\,(2x_1/b - 1) \tag{84}$$

Again an excellent match is observed in the validation study.

Figures 13, 14, and 15 present the results for the contact stresses $\sigma_{22}(x_1, 0)$ for the wedge-shaped punch. The contact pressure $\sigma_{22}(x_1, 0)$ is bounded at the smooth edge $x_1 = b$ and singular at the sharp edge $x_1 = 0$. In Fig. 13, contact pressure distribution for different values of the inhomogeneity parameter is plotted in the range $0 \leq \beta b \leq 4$ for different values of the shear parameter, κ, and the coefficient of friction η. When the inhomogeneity parameter βb approaches to zero, we should recover the orthotropic homogeneous results of Ref. [58]. This validation can be seen in Fig. 13a. In order to be consistent with the direction of the lateral force Q taken in Ref. [58], the coefficient of friction is taken to be negative. Note that the effect of the coefficient of friction, η, is significant for small values of the shear parameter κ. For reference, one can see the effect of the inhomogeneity parameter on the contact stresses for fixed values of the coefficient of friction ($\eta = 0, -0.9$)

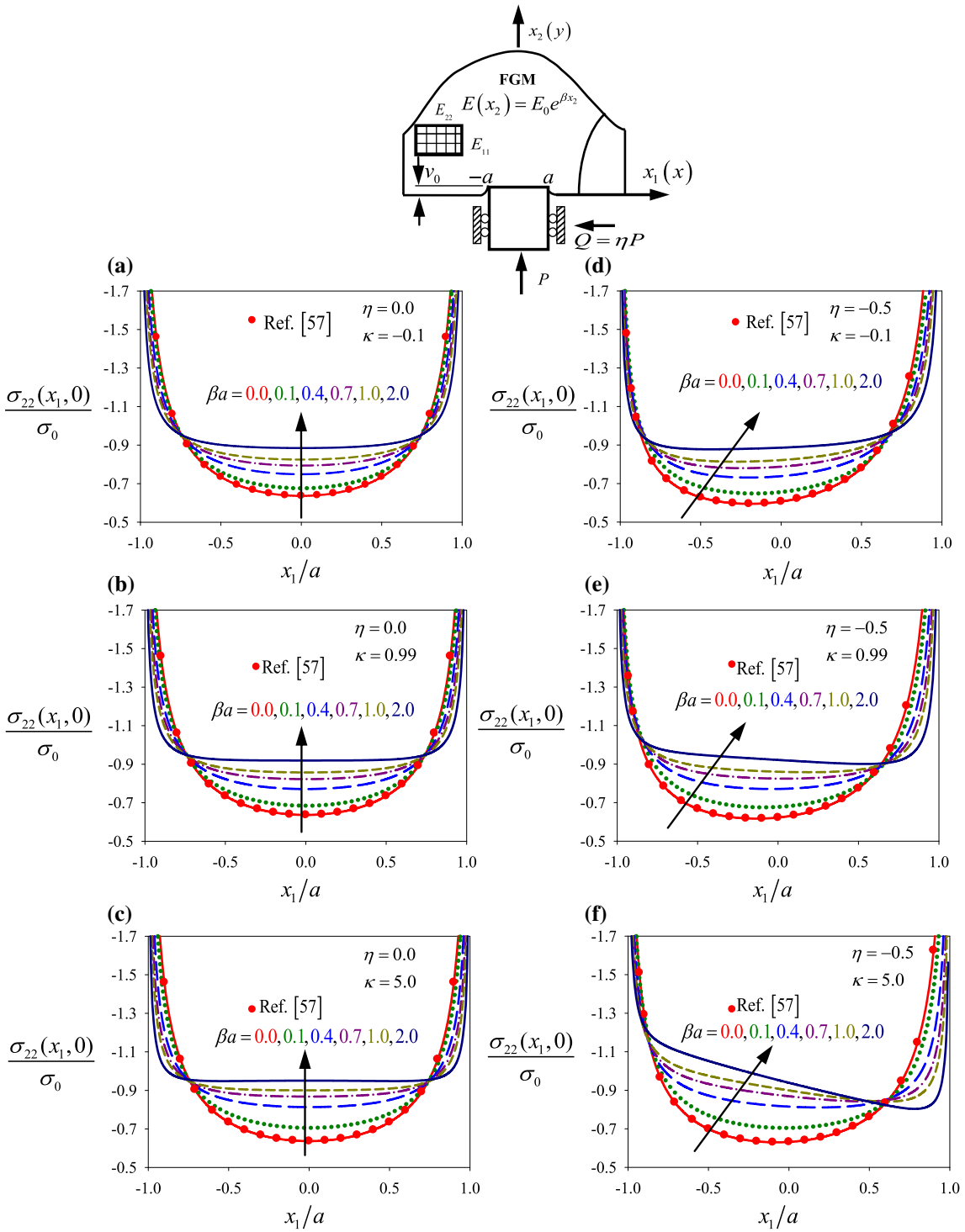

Fig. 6 Contact pressure distribution, $\sigma_{22}(x_1, 0)$, at the surface of graded orthotropic half-plane loaded by a flat stamp for various values of the inhomogeneity parameter, βa, with the parameters $\nu = 3/7$, $\delta^4 = 0.2$, $\sigma_0 = \frac{P}{2a}$, **a** $\eta = 0.0$, $\kappa = -0.1$, **b** $\eta = 0.0$, $\kappa = 0.99$, **c** $\eta = 0.0$, $\kappa = 5.0$, **d** $\eta = -0.5$, $\kappa = -0.1$, **e** $\eta = -0.5$, $\kappa = 0.99$, **f** $\eta = -0.5$, $\kappa = 5.0$

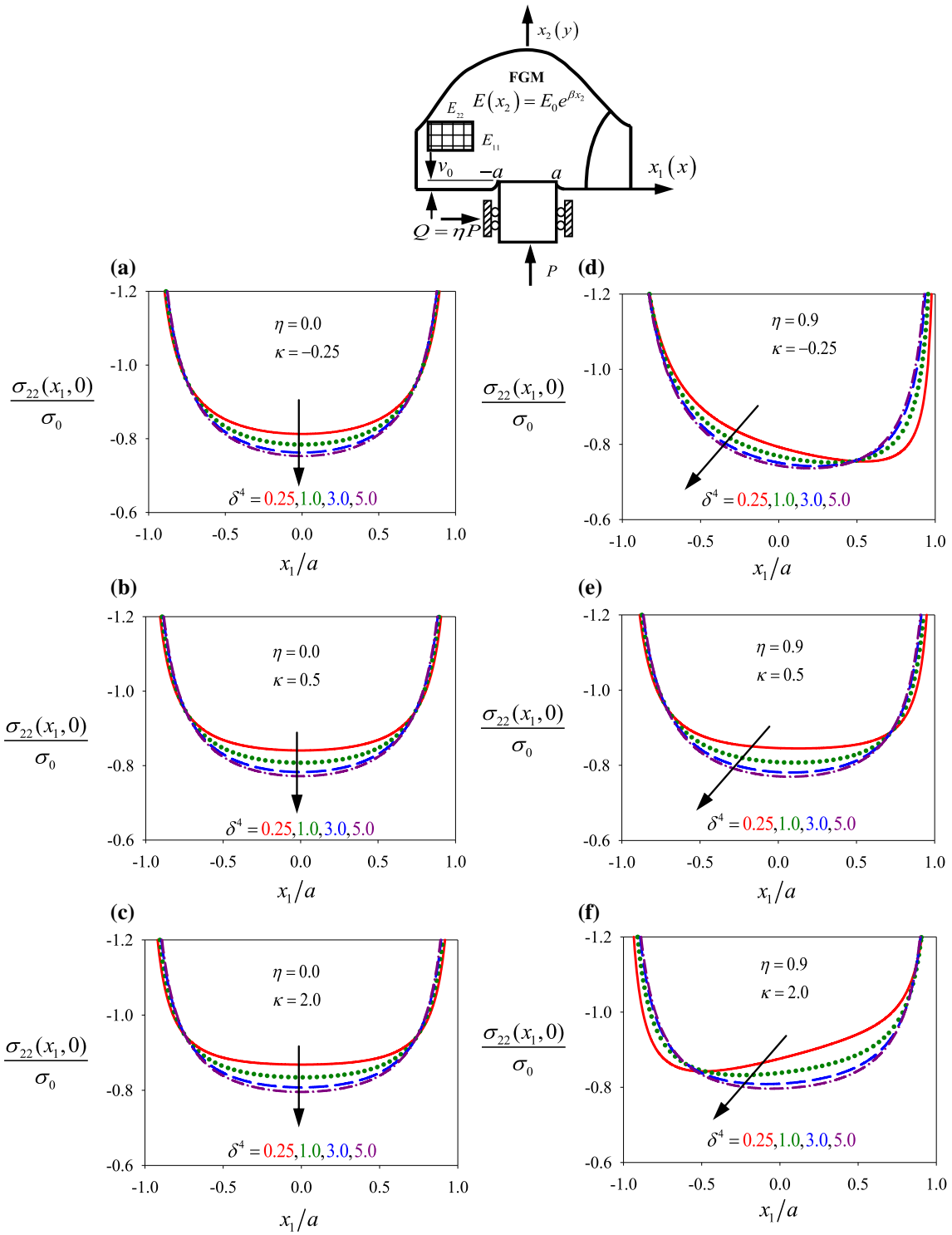

Fig. 7 Contact pressure distribution, $\sigma_{22}(x_1, 0)$, at the surface of graded orthotropic half-plane loaded by a flat stamp for various values of the stiffness ratio, δ, with the parameters $\beta a = 1.0$, $\nu = 3/7$, $\sigma_0 = \frac{P}{2a}$, **a** $\eta = 0.0$, $\kappa = -0.25$, **b** $\eta = 0.0$, $\kappa = 0.5$, **c** $\eta = 0.0$, $\kappa = 2.0$, **d** $\eta = 0.9$, $\kappa = -0.25$, **e** $\eta = 0.9$, $\kappa = 0.5$, **f** $\eta = 0.9$, $\kappa = 2.0$

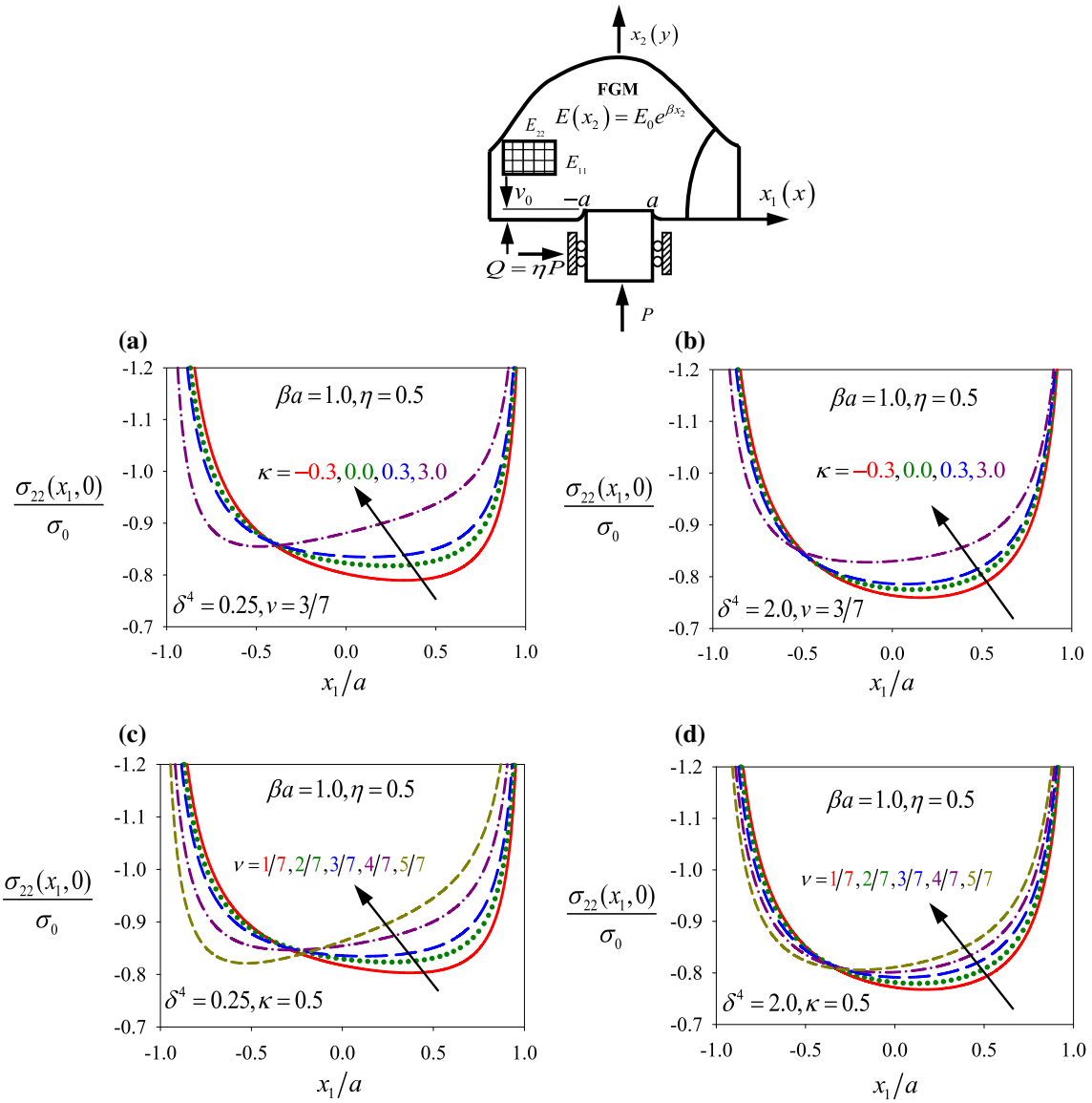

Fig. 8 Contact pressure, $\sigma_{22}(x_1, 0)$, distribution at the surface of graded orthotropic half-plane loaded by a flat stamp for various values of the shear parameter, κ, and the effective Poisson' s ratio, ν, with the parameters $\beta a = 1.0$, $\eta = 0.5$, $\sigma_0 = \frac{P}{2a}$, **a** $\delta^4 = 0.25$, $\nu = 3/7$, **b** $\delta^4 = 2.0$, $\nu = 3/7$, **c** $\delta^4 = 0.25$, $\kappa = 0.5$, **d** $\delta^4 = 2.0$, $\kappa = 0.5$

in Fig. 14. The effect of the stiffness ratio for various values of the coefficient of friction and shear parameter can be seen in Fig. 15.

The distribution of the in-plane stress component for wedge-shaped stamp is shown in Fig. 16 for $\eta < 0$. It can be seen that the in-plane stresses have a tensile peak at the trailing edge of the contact which might be responsible for crack initiation or surface damage. Figure 17 shows the behavior of the in-plane stress component when $\eta > 0$ and note that the in-plane stresses are tensile at the trailing region of the contact.

Finally, Fig. 18 depicts the load versus the contact length distributions, P, for various values of the coefficient of friction. The figure shows that the effect of coefficient of friction η on the P is quite significant.

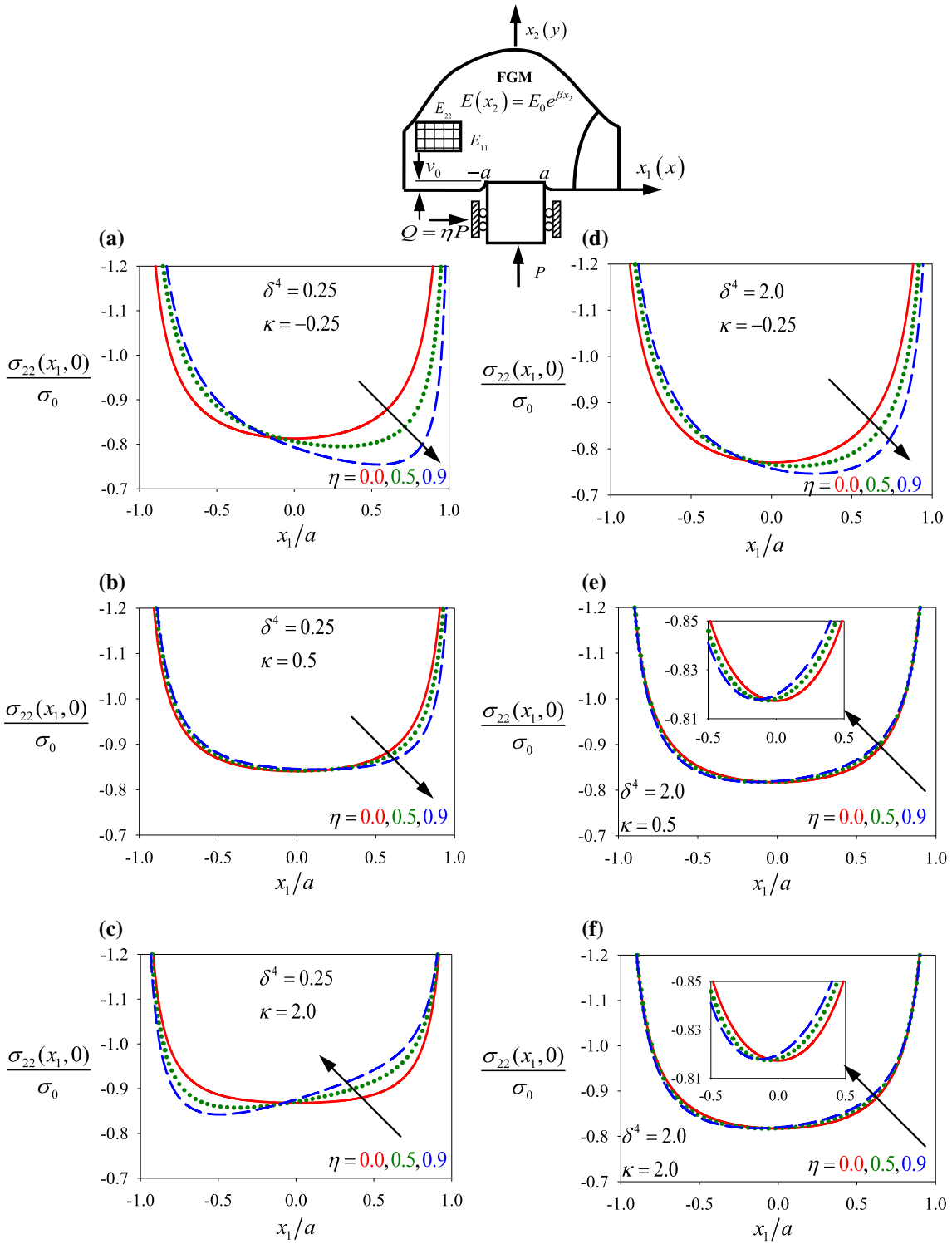

Fig. 9 Contact pressure, $\sigma_{22}(x_1, 0)$, distribution at the surface of graded orthotropic half-plane loaded by a flat stamp for various values of the friction coefficient, η, with the parameters $\beta a = 1.0$, $\nu = 3/7$, $\sigma_0 = \frac{P}{2a}$, **a** $\kappa = -0.25$, $\delta^4 = 0.25$, **b** $\kappa = 0.5$, $\delta^4 = 0.25$, **c** $\kappa = 2.0$, $\delta^4 = 0.25$, **d** $\kappa = -0.25$, $\delta^4 = 2.0$, **e** $\kappa = 0.5$, $\delta^4 = 2.0$, **f** $\kappa = 2.0$, $\delta^4 = 2.0$

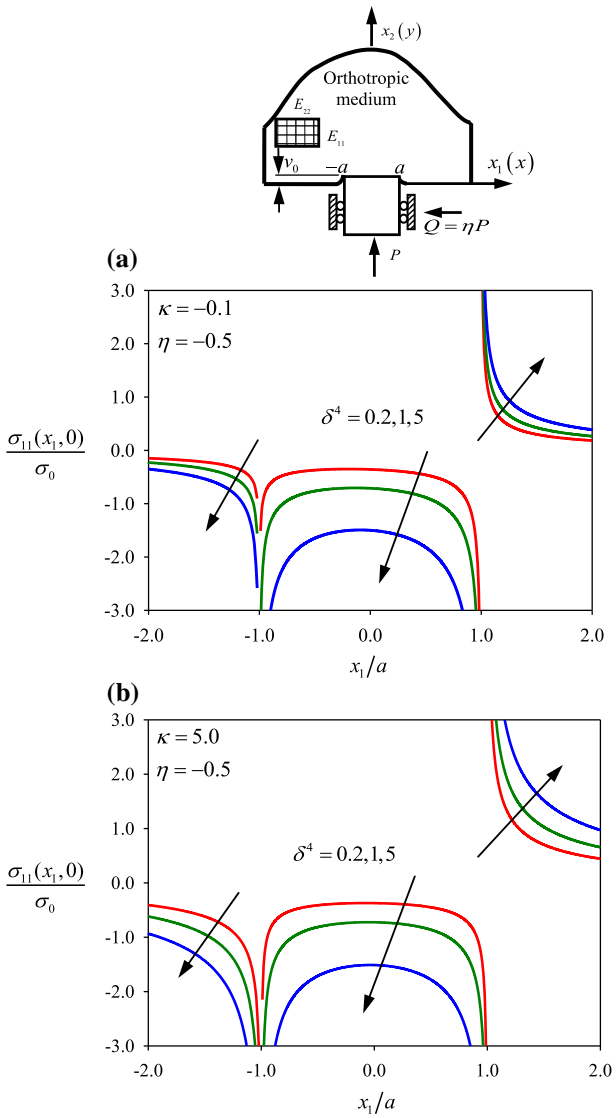

Fig. 10 In-plane stress, $\sigma_{11}(x_1, 0)$, distribution at the surface of homogeneous orthotropic half-plane loaded by a flat stamp for various values of the stiffness ratio, δ, with the parameters $\nu = 3/7$, $\eta = -0.5$, $\sigma_0 = \frac{P}{2a}$, **a** $\kappa = -0.1$, **b** $\kappa = 5.0$

8 Concluding remarks

In this study, analytical and numerical methods are developed to determine contact stress distributions in orthotropic graded materials that are subjected to frictional contact by a rigid stamp with arbitrary profile. Two different profiles (flat and wedge type) are used for the numerical results presented in Sect. 6. Below, we summarize the major findings of this study.

- The results obtained in this study are in excellent agreement with the limiting cases (isotropic graded results of Ref. [67], orthotropic homogeneous results of Ref. [57] for flat stamp, and orthotropic homogeneous results of Ref. [58] for wedge stamp. Therefore, this study can be used as benchmark results for the contact stresses involving orthotropic graded materials.
- The weight functions describing the asymptotic behavior of the contact stresses are dependent on the coefficient of friction and the value of effective Poisson's ratio and the shear parameter only, and are independent of all other material constants and length parameters. As shown in the formulation section, the leading term in the asymptotic solution is evaluated in closed form.

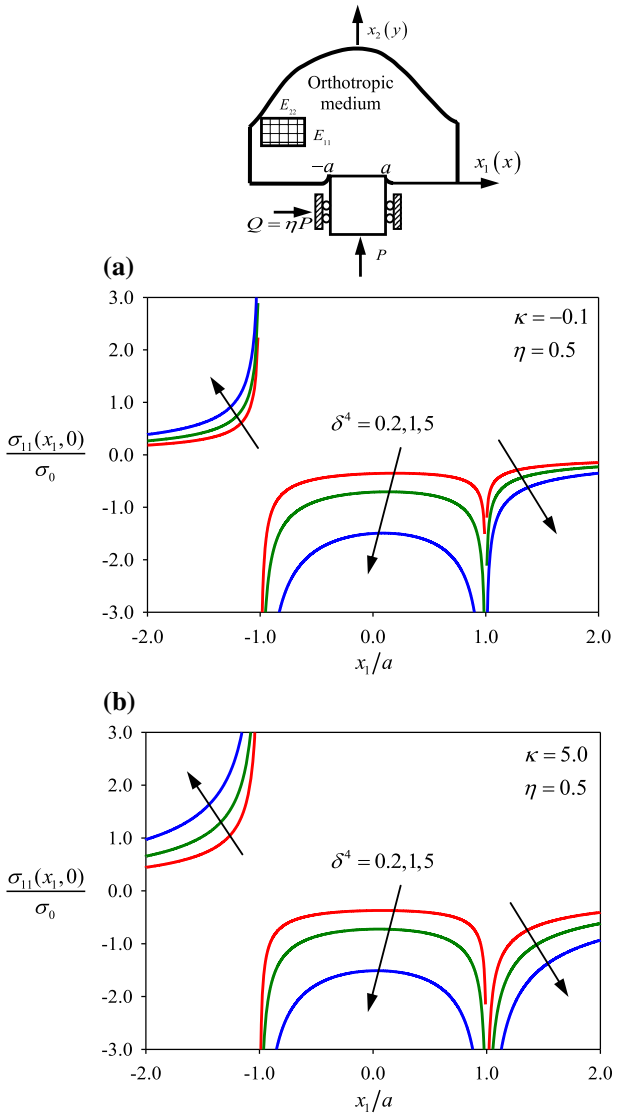

Fig. 11 In-plane stress, $\sigma_{11}(x_1, 0)$, distribution at the surface of homogeneous orthotropic half-plane loaded by a flat stamp for various values of the stiffness ratio, δ, with the parameters $\nu = 3/7$, $\eta = 0.5$, $\sigma_0 = \frac{P}{2a}$, **a** $\kappa = -0.1$, **b** $\kappa = 5.0$

- As the coefficient of friction increases, the contact pressure curves slant toward the leading edge when the shear parameter, κ, is less than one and to the trailing edge when the shear parameter is greater than one.
- As in the crack problems for graded materials (see [65]), the shear parameter, κ, has a significant effect on the contact pressure distribution, especially when $\kappa < 0$.
- For wedge-shaped stamp, the in-plane stress component has a tensile peak at the trailing edge of the component and may be responsible for surface damage and crack initiation at trailing edge of the contact.
- Orthotropic graded materials are shown to possess the potential to be used to lower the stress levels in the contact surfaces that are susceptible for crack initiation due to frictional contact.

The theory proposed in this paper possesses application to several contact problems related to orthotropic materials. For example, the theory can be further extended to cover the contact mechanics of orthotropic magneto-electro-elastic materials (MEEMs) or orthotropic functionally graded magneto-electro-elastic materials (FGMEEMs). Sensors, actuators, optoelectronic devices, storage devices, and electronic instrumentations are among the current applications of MEEMs. In order to characterize the mechanical, electric, and magnetic performance, the mechanics of contact for these materials has to be fully understood (see, for example, [68,69]).

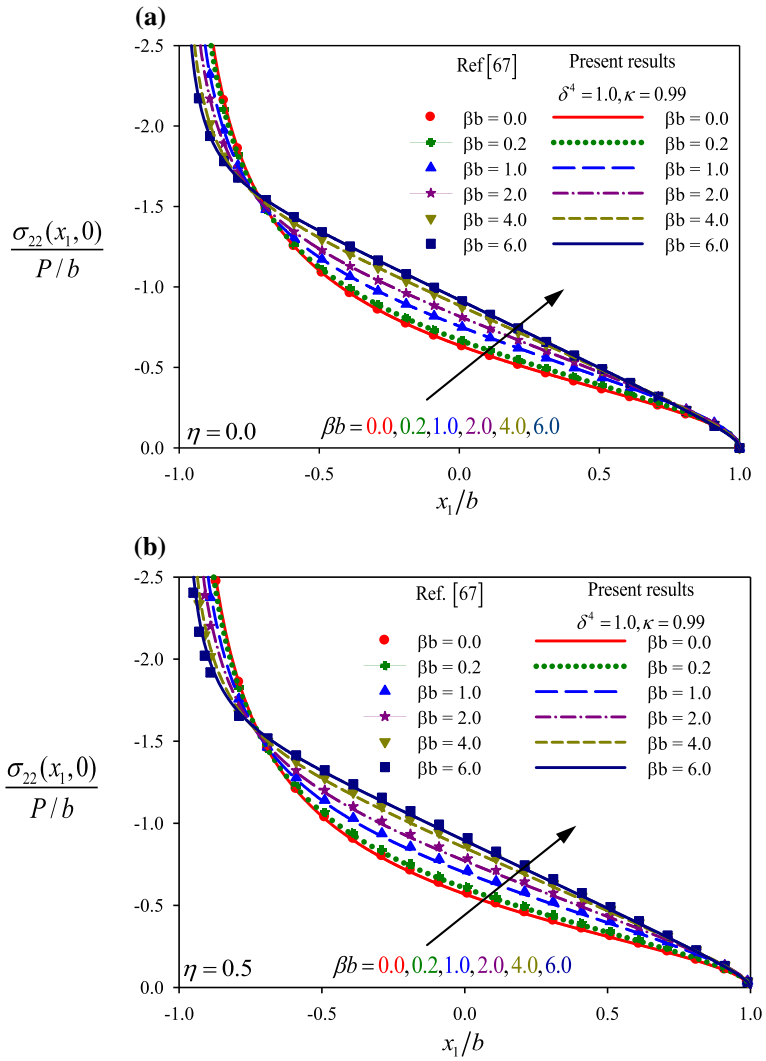

Fig. 12 Contact pressure, $\sigma_{22}(x_1, 0)$, distribution at the surface of graded orthotropic half-plane loaded by a wedge stamp for various values of the inhomogeneity parameter, βb, with the parameters, $\kappa = 0.99$, $\delta^4 = 1.0$, $\nu = 3/7$, $\sigma_0 = \frac{P}{b}$, **a** $\eta = 0.0$, **b** $\eta = 0.5$

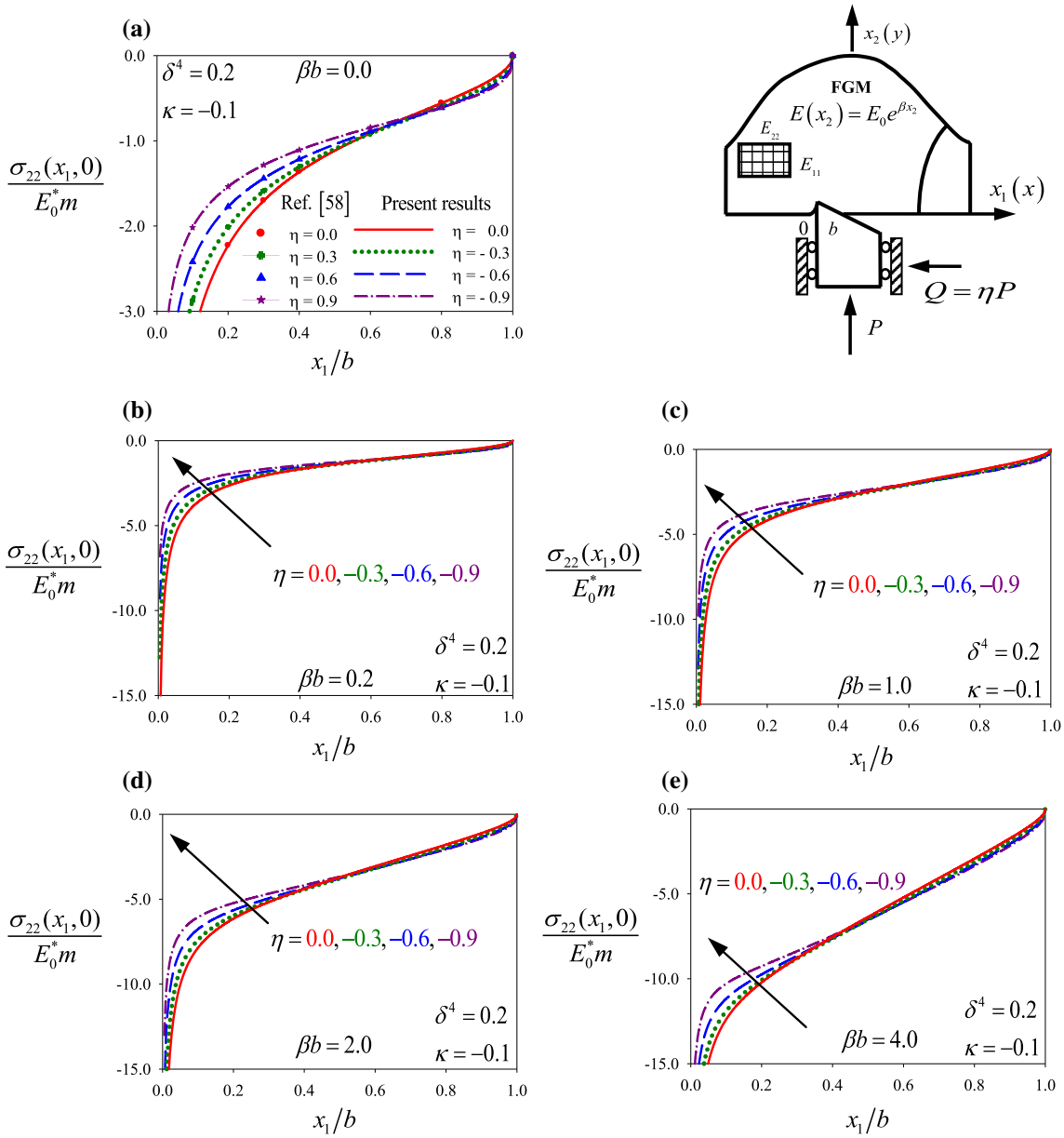

Fig. 13 Contact pressure, $\sigma_{22}(x_1, 0)$, distribution at the surface of graded orthotropic half-plane loaded by a wedge stamp for various values of the friction coefficient, η, with the parameters $\delta^4 = 0.2$, $\kappa = -0.1$, $\nu = 3/7$, **a** $\beta b = 0.0$, **b** $\beta b = 0.2$, **c** $\beta b = 1.0$, **d** $\beta b = 2.0$, **e** $\beta b = 4.0$, where E_0^* is given in Eq. (9c)

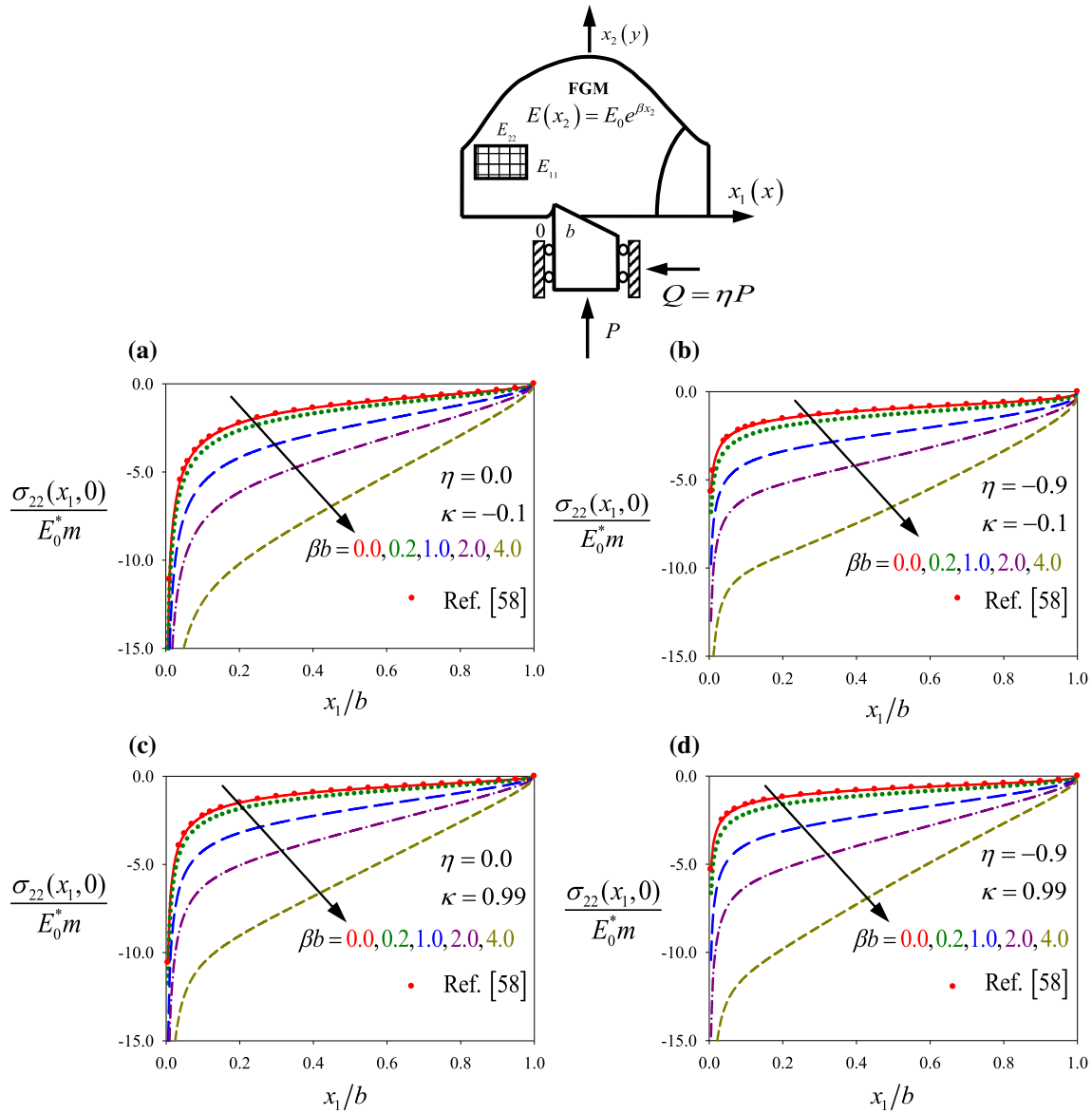

Fig. 14 Contact pressure, $\sigma_{22}(x_1, 0)$, distribution at the surface of graded orthotropic half-plane loaded by a wedge stamp for various values of the inhomogeneity parameter, βb, with the parameters $\nu = 3/7$, $\delta^4 = 0.2$, **a** $\eta = 0.0$, $\kappa = -0.1$, **b** $\eta = -0.9$, $\kappa = -0.1$, **c** $\eta = 0.0$, $\kappa = 0.99$, **d** $\eta = -0.9$, $\kappa = 0.99$ where E_0^* is given in Eq. (9c)

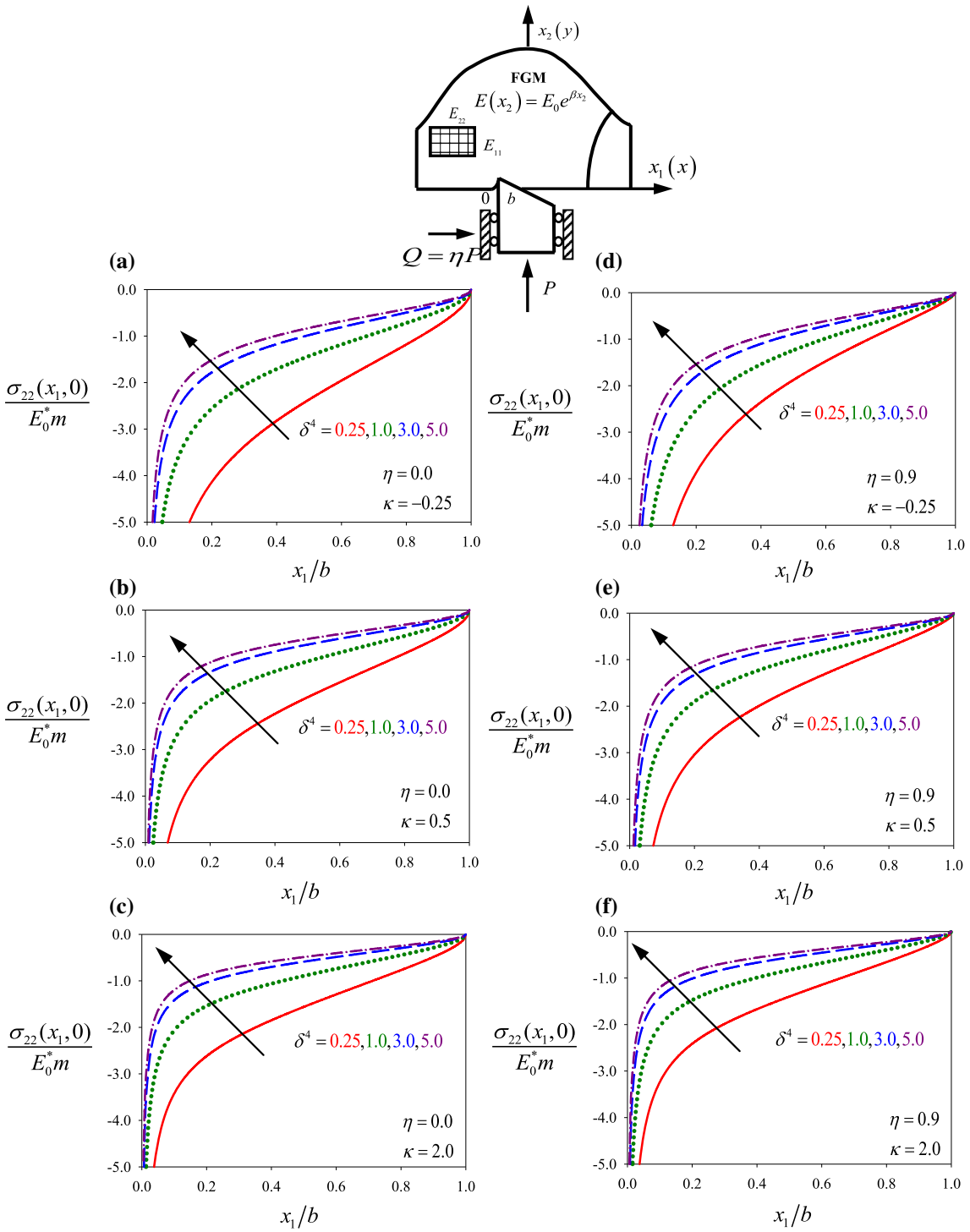

Fig. 15 Contact pressure, $\sigma_{22}(x_1, 0)$, distribution at the surface of graded orthotropic half-plane loaded by a wedge stamp for various values of the stiffness ratio, δ, with the parameters $\beta b = 1.0$, $\nu = 3/7$, **a** $\kappa = -0.25$, $\eta = 0.0$, **b** $\kappa = 0.5$, $\eta = 0.0$, **c** $\kappa = 2.0$, $\eta = 0.0$, **d** $\kappa = -0.25$, $\eta = 0.9$, **e** $\kappa = 0.5$, $\eta = 0.9$, **f** $\kappa = 2.0$, $\eta = 0.9$, where E_0^* is given in Eq. (9c)

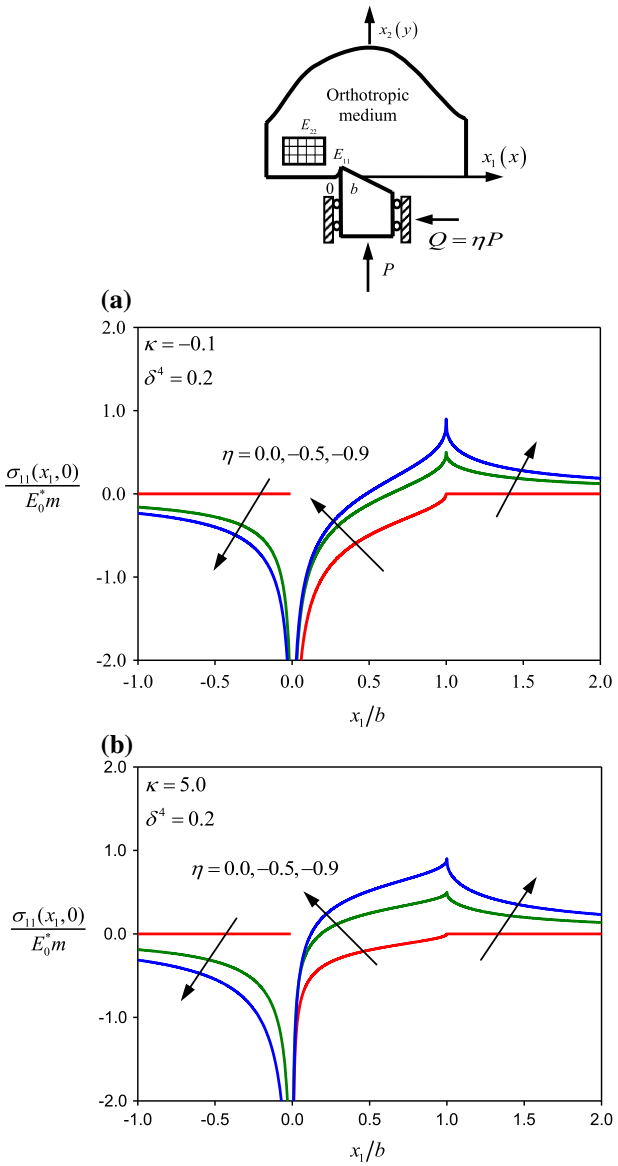

Fig. 16 In-plane stress, $\sigma_{11}(x_1, 0)$, distribution at the surface of homogeneous orthotropic half-plane loaded by a wedge stamp for various values of the coefficient of friction, $\eta \leq 0$, with the parameters $\nu = 3/7$, $\delta^4 = 0.2$, **a** $\kappa = -0.1$, **b** $\kappa = 5.0$, where E_0^* is given in Eq. (9c)

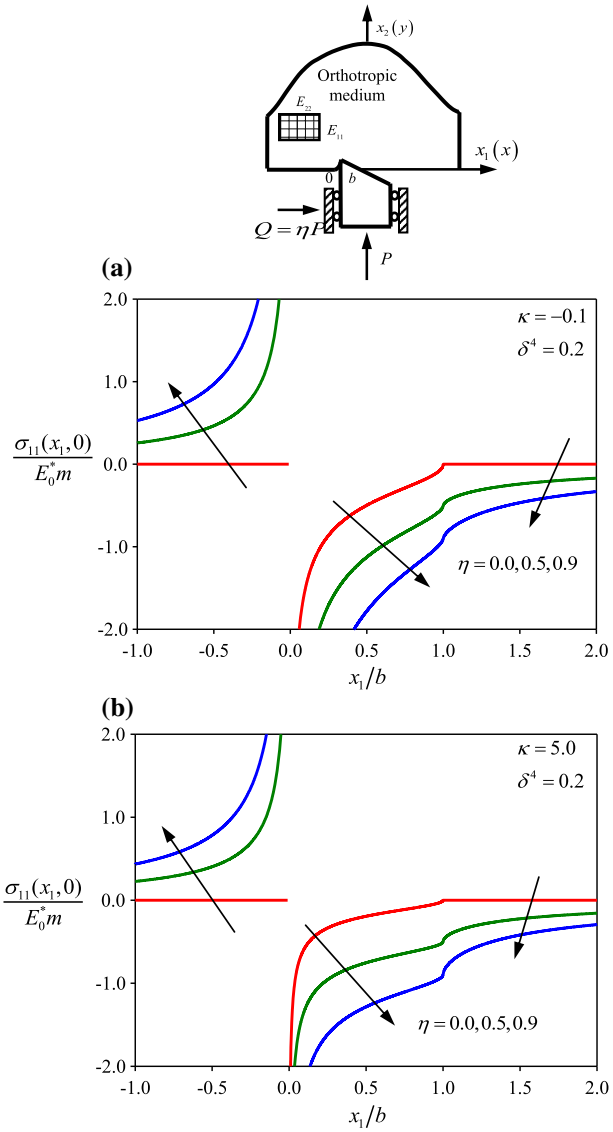

Fig. 17 In-plane stress, $\sigma_{11}(x_1, 0)$, distribution at the surface of homogeneous orthotropic half-plane loaded by a wedge stamp for various values of the coefficient of friction, $\eta \geq 0$, with the parameters $\nu = 3/7$, $\delta^4 = 0.2$, **a** $\kappa = -0.1$, **b** $\kappa = 5.0$, where E_0^* is given in Eq. (9c)

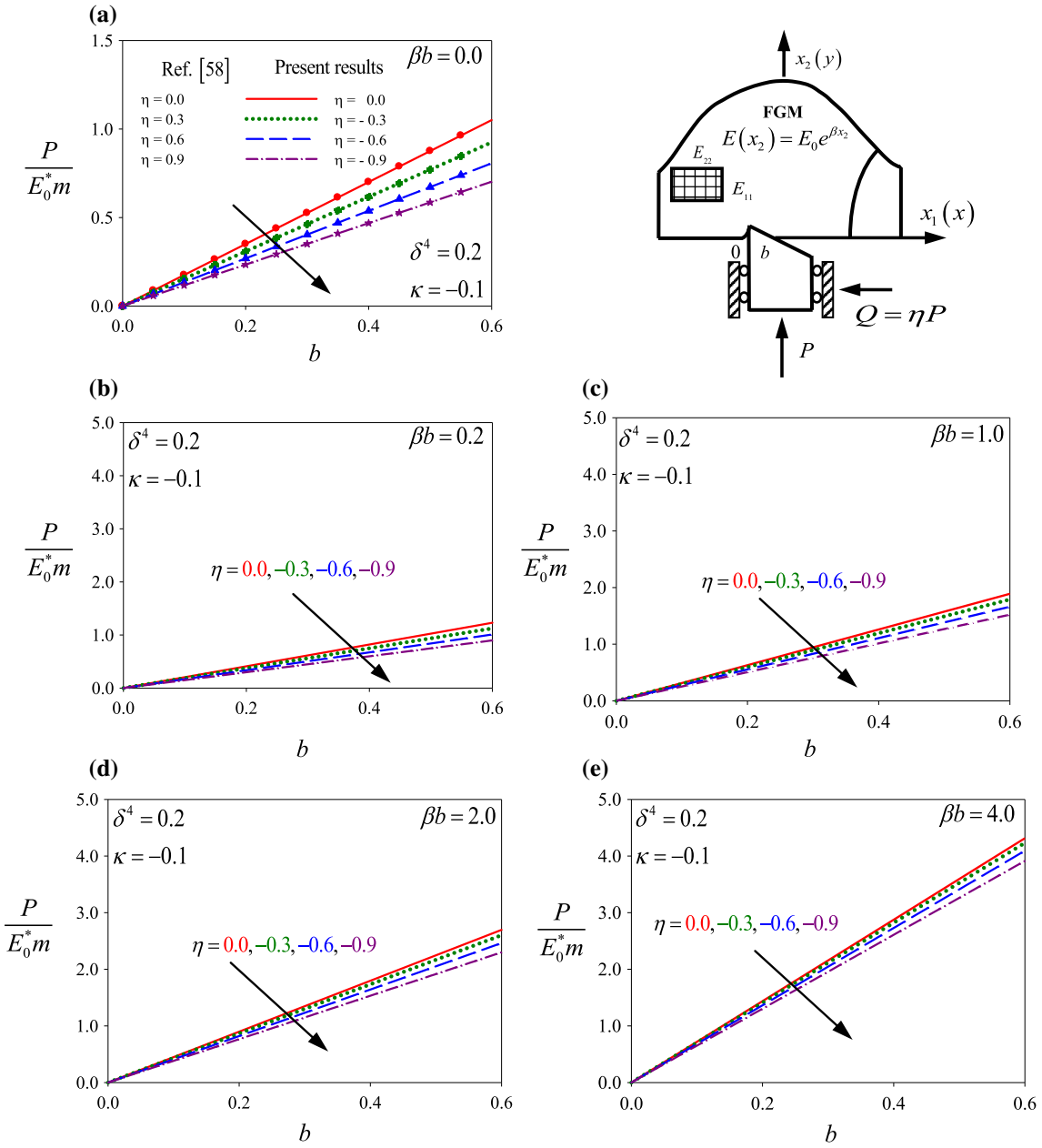

Fig. 18 Load versus the contact length distributions, P, for graded orthotropic half-plane loaded by a wedge stamp for various values of the coefficient ratio, η, with the parameters $\delta^4 = 0.2$, $\kappa = -0.1$, $\nu = 3/7$, **a** $\beta b = 0.0$, **b** $\beta b = 0.2$, **c** $\beta b = 1.0$, **d** $\beta b = 2.0$, **e** $\beta b = 4.0$, where E_0^* is given in Eq. (9c)

Acknowledgments The author (A.K.) would like to thank the Scientific and Technological Research Council of Turkey (TUBITAK) for funding this research through the program BIDEB—2218 "Postgraduate Research Fellowship" during her postgraduate studies at TOBB University of Economics and Technology.

Appendix A: The roots of the characteristic equation (14)

Depending on the values of κ, there are three cases of the characteristic roots of Eq. (14):
Case A: $-1 < \kappa < \sqrt{1+\nu\left(\frac{\gamma}{\alpha}\right)^2}$, two pairs of complex conjugate roots:

$$n_1 = |\alpha|\left(-\frac{\gamma}{2|\alpha|}+\sqrt{\left(\frac{\gamma}{2|\alpha|}\right)^2+\kappa+i\chi_1}\right)=\overline{n_3},\quad \Re e\,(n_1,n_3)>0, \tag{A.1}$$

$$n_2 = |\alpha|\left(-\frac{\gamma}{2|\alpha|}-\sqrt{\left(\frac{\gamma}{2|\alpha|}\right)^2+\kappa+i\chi_1}\right)=\overline{n_4},\quad \Re e\,(n_2,n_4)<0, \tag{A.2}$$

$$\chi_1=\sqrt{1-\kappa^2+\nu\left(\frac{\gamma}{\alpha}\right)^2}; \tag{A.3}$$

Case B: $\kappa > \sqrt{1+\nu\left(\frac{\gamma}{\alpha}\right)^2}$, four distinct real roots:

$$n_1 = |\alpha|\left(-\frac{\gamma}{2|\alpha|}+\sqrt{\left(\frac{\gamma}{2|\alpha|}\right)^2+\kappa-\chi_1}\right),\quad \Re e\,(n_1)>0, \tag{A.4}$$

$$n_2 = |\alpha|\left(-\frac{\gamma}{2|\alpha|}-\sqrt{\left(\frac{\gamma}{2|\alpha|}\right)^2+\kappa-\chi_1}\right),\quad \Re e\,(n_2)<0, \tag{A.5}$$

$$n_3 = |\alpha|\left(-\frac{\gamma}{2|\alpha|}+\sqrt{\left(\frac{\gamma}{2|\alpha|}\right)^2+\kappa+\chi_1}\right),\quad \Re e\,(n_3)>0, \tag{A.6}$$

$$n_4 = |\alpha|\left(-\frac{\gamma}{2|\alpha|}-\sqrt{\left(\frac{\gamma}{2|\alpha|}\right)^2+\kappa+\chi_1}\right),\quad \Re e\,(n_4)<0, \tag{A.7}$$

$$\chi_1=\sqrt{\kappa^2-1-\nu\left(\frac{\gamma}{\alpha}\right)^2}; \tag{A.8}$$

Case C: $\kappa = \sqrt{1+\nu\left(\frac{\gamma}{\alpha}\right)^2}$, two real double roots:

$$n_1 = |\alpha|\left(-\frac{\gamma}{2|\alpha|}+\sqrt{\left(\frac{\gamma}{2|\alpha|}\right)^2+\kappa}\right)=n_3,\quad \Re e\,(n_1,n_3)>0, \tag{A.9}$$

$$n_2 = |\alpha|\left(-\frac{\gamma}{2|\alpha|}-\sqrt{\left(\frac{\gamma}{2|\alpha|}\right)^2+\kappa}\right)=n_4,\quad \Re e\,(n_2,n_4)<0. \tag{A.10}$$

Note that when $\kappa \to 1$ and $\delta^4 \to 1$, we must recover the isotropic infinitely graded half-plane formulation. Observe that this situation corresponds to case 1 where $-1 < \kappa < \sqrt{1+\nu\left(\frac{\gamma}{\alpha}\right)^2}$. Therefore, for this special case of the problem, the roots become

$$n_1^{\text{iso}} = |\alpha| \left(-\frac{\gamma}{2|\alpha|} + \sqrt{\left(\frac{\gamma}{2|\alpha|}\right)^2 + 1 + i\frac{|\gamma|}{|\alpha|}\delta_0} \right), \quad \Re e\,(n_1) > 0, \tag{A.11}$$

$$n_2^{\text{iso}} = |\alpha| \left(-\frac{\gamma}{2|\alpha|} - \sqrt{\left(\frac{\gamma}{2|\alpha|}\right)^2 + 1 + i\frac{|\gamma|}{|\alpha|}\delta_0} \right), \quad \Re e\,(n_2) < 0, \tag{A.12}$$

$$n_3^{\text{iso}} = |\alpha| \left(-\frac{\gamma}{2|\alpha|} + \sqrt{\left(\frac{\gamma}{2|\alpha|}\right)^2 + 1 - i\frac{|\gamma|}{|\alpha|}\delta_0} \right), \quad \Re e\,(n_3) > 0, \tag{A.13}$$

$$n_4^{\text{iso}} = |\alpha| \left(-\frac{\gamma}{2|\alpha|} - \sqrt{\left(\frac{\gamma}{2|\alpha|}\right)^2 + 1 - i\frac{|\gamma|}{|\alpha|}\delta_0} \right), \quad \Re e\,(n_4) < 0, \tag{A.14}$$

where

$$\delta_0 = \begin{cases} \sqrt{\nu_0} & \text{generalized plane stress conditions} \\ \sqrt{\frac{1}{1-\nu_0}} & \text{plane strain conditions} \end{cases} \tag{A.15}$$

and ν_0 being the Poisson's ratio of the corresponding isotropic half-plane.

Appendix B: The asymptotic analysis of the kernels in the integral equation

In Sect. 2, the formulation of the ordinary stress boundary value problem shown in Fig. 2 is described. The frictional contact problems given in Fig. 1 are mixed boundary value problems in which the contact stresses σ, τ are zero outside the contact region, $x_1 < -a$, $x_1 > b$, and displacement components are defined in the contact region $-a < x_1 < b$ through the given stamp profile. Taking the x-derivative of Eqs. (11a) and (11b), the displacement derivatives on the surface of the orthotropic graded half-plane can be expressed as:

$$\begin{aligned} &\lim_{y\to 0} \pi E_0^* \frac{\mathrm{d}}{\mathrm{d}x} v(x, y), \\ &= \lim_{y\to 0} \int_{-\infty}^{\infty} K_{11}(x, y, t)\sigma_{yy}(t, y)\,\mathrm{d}t + \lim_{y\to 0} \int_{-\infty}^{\infty} K_{12}(x, y, t)\sigma_{xy}(t, y)\,\mathrm{d}t, \end{aligned} \tag{B.1}$$

$$\begin{aligned} &\lim_{y\to 0} \pi E_0^* \frac{\mathrm{d}}{\mathrm{d}x} u(x, y) \\ &= \lim_{y\to 0} \int_{-\infty}^{\infty} K_{21}(x, y, t)\sigma_{yy}(t, y)\,\mathrm{d}t + \lim_{y\to 0} \int_{-\infty}^{\infty} K_{22}(x, y, t)\sigma_{xy}(t, y)\,\mathrm{d}t, \end{aligned} \tag{B.2}$$

where the kernels $K_{ij}(x, y, t)$ $(i, j = 1, 2)$ are known functions (see [62] for details), and to dictate the nature of singularity coming from the Cauchy singularities and delta functions, Eqs. (B.1) and (B.2) are expressed in terms of displacement derivatives rather than displacements. The kernels $K_{ij}(x, y, t)$ $(i, j = 1, 2)$ can be expressed as:

$$K_{ij}(x, y, t) = \int_{-\infty}^{\infty} H_{ij}(\alpha, y)\mathrm{e}^{-i\alpha(t-x)}\mathrm{d}\alpha \quad (i, j = 1, 2), \tag{B.3}$$

where

$$H_{11}(\alpha, y) = -\frac{i\alpha}{\Delta_0(\alpha)}\left[\frac{(1-\nu^2)}{2}\left(\bar{Z}_2(\alpha)\mathrm{e}^{n_2 y} + Z_2(\alpha)\mathrm{e}^{n_4 y}\right)\right], \tag{B.4}$$

$$H_{21}(\alpha, y) = -\frac{i\alpha}{\Delta_0(\alpha)}\left[\frac{(1-\nu^2)}{2}\left(A_2\bar{Z}_2(\alpha)\mathrm{e}^{n_2 y} - \bar{A}_2 Z_2(\alpha)\mathrm{e}^{n_4 y}\right)\right], \tag{B.5}$$

$$H_{12}(\alpha, y) = -\frac{i\alpha}{\Delta_0(\alpha)}\left[(\kappa+\nu)\left(\bar{Z}_1(\alpha)\mathrm{e}^{n_2 y} - Z_1(\alpha)\mathrm{e}^{n_4 y}\right)\right], \tag{B.6}$$

$$H_{22}(\alpha, y) = -\frac{i\alpha}{\Delta_0(\alpha)}\left[(\kappa+\nu)\left(A_2(\alpha)\bar{Z}_1(\alpha)\mathrm{e}^{n_2 y} + \bar{A}_2(\alpha)Z_1(\alpha)\mathrm{e}^{n_4 y}\right)\right]. \tag{B.7}$$

Singularities in the kernels are dictated by the asymptotic behavior of integrands. Asymptotic analysis as $\alpha \to \infty$ must be done to extract the singularities. As $\alpha \to \infty$, asymptotic behavior of $H_{11}(\alpha, y)$, $H_{12}(\alpha, y)$, $H_{21}(\alpha, y)$ and $H_{22}(\alpha, y)$ can be obtained as:

$$\begin{aligned} H_{11}(\alpha, y) = {} & \frac{i\alpha}{|\alpha|}\left[a_{10} + a_{11}\frac{\gamma}{|\alpha|} + \mathrm{O}\left(\frac{1}{\alpha^2}\right)\right]\mathrm{e}^{-r_1|\alpha|y} \\ & + \frac{i\alpha}{|\alpha|}\left[a_{20} + a_{21}\frac{\gamma}{|\alpha|} + \mathrm{O}\left(\frac{1}{\alpha^2}\right)\right]\mathrm{e}^{-r_2|\alpha|y}, \end{aligned} \tag{B.8}$$

$$\begin{aligned} H_{21}(\alpha, y) = {} & \left[b_{10} + b_{11}\frac{\gamma}{|\alpha|} + \mathrm{O}\left(\frac{1}{\alpha^2}\right)\right]\mathrm{e}^{-r_1|\alpha|y} \\ & + \left[b_{20} + b_{21}\frac{\gamma}{|\alpha|} + \mathrm{O}\left(\frac{1}{\alpha^2}\right)\right]\mathrm{e}^{-r_2|\alpha|y}, \end{aligned} \tag{B.9}$$

$$\begin{aligned} H_{12}(\alpha, y) = {} & \left[c_{10} + c_{11}\frac{\gamma}{|\alpha|} + \mathrm{O}\left(\frac{1}{\alpha^2}\right)\right]\mathrm{e}^{-r_1|\alpha|y} \\ & + \left[c_{20} + c_{21}\frac{\gamma}{|\alpha|} + \mathrm{O}\left(\frac{1}{\alpha^2}\right)\right]\mathrm{e}^{-r_2|\alpha|y}, \end{aligned} \tag{B.10}$$

$$\begin{aligned} H_{22}(\alpha, y) = {} & \frac{i\alpha}{|\alpha|}\left[d_{10} + d_{11}\frac{\gamma}{|\alpha|} + \mathrm{O}\left(\frac{1}{\alpha^2}\right)\right]\mathrm{e}^{-r_1|\alpha|y} \\ & + \frac{i\alpha}{|\alpha|}\left[d_{20} + d_{21}\frac{\gamma}{|\alpha|} + \mathrm{O}\left(\frac{1}{\alpha^2}\right)\right]\mathrm{e}^{-r_2|\alpha|y}, \end{aligned} \tag{B.11}$$

where

$$a_{10} + a_{20} = a_0 = \kappa_1\frac{r_1 r_2}{r_1 - r_2}, \tag{B.12}$$

$$b_{10} + b_{20} = b_0 = \frac{1}{2}\frac{r_2 r_3 - r_1 r_4}{r_1 - r_2}, \tag{B.13}$$

$$c_{10} + c_{20} = c_0 = \frac{1}{2}\frac{r_1 r_4 - r_2 r_3}{r_1 - r_2}, \tag{B.14}$$

$$d_{10} + d_{20} = d_0 = \frac{\kappa_1}{r_1 - r_2}, \tag{B.15}$$

$$\kappa_1 = i\sqrt{1-\kappa^2}, \tag{B.16}$$

$$r_1 = \sqrt{\kappa - \kappa_1}, \tag{B.17}$$

$$r_2 = \sqrt{\kappa + \kappa_1}, \tag{B.18}$$

$$r_3 = \kappa + \nu - \kappa_1, \tag{B.19}$$

$$r_4 = \kappa + \nu + \kappa_1. \tag{B.20}$$

Examining the asymptotic behavior of $H_{ij}(\alpha, y)$ $(i, j = 1, 2)$, the asymptotic terms in Eq. (B.3) can be obtained as (see [62] for details)

$$K_{11\infty} = i a_{10} \int_{-\infty}^{\infty} \frac{\alpha}{|\alpha|} e^{-r_1|\alpha|y} e^{-i\alpha(t-x)} d\alpha + i a_{20} \int_{-\infty}^{\infty} \frac{\alpha}{|\alpha|} e^{-r_2|\alpha|y} e^{-i\alpha(t-x)} d\alpha$$
$$= a_{10} \frac{2(t-x)}{r_1^2 y^2 + (t-x)^2} + a_{20} \frac{2(t-x)}{r_2^2 y^2 + (t-x)^2}, \tag{B.21}$$

$$K_{21\infty} = b_{10} \int_{-\infty}^{\infty} e^{-r_1|\alpha|y} e^{-i\alpha(t-x)} d\alpha + b_{20} \int_{-\infty}^{\infty} e^{-r_2|\alpha|y} e^{-i\alpha(t-x)} d\alpha$$
$$= b_{10} \frac{2y}{r_1^2 y^2 + (t-x)^2} + b_{20} \frac{2y}{r_2^2 y^2 + (t-x)^2}, \tag{B.22}$$

$$K_{12\infty} = c_{10} \int_{-\infty}^{\infty} e^{-r_1|\alpha|y} e^{-i\alpha(t-x)} d\alpha + c_{20} \int_{-\infty}^{\infty} e^{-r_2|\alpha|y} e^{-i\alpha(t-x)} d\alpha$$
$$= c_{10} \frac{2y}{r_1^2 y^2 + (t-x)^2} + c_{20} \frac{2y}{r_2^2 y^2 + (t-x)^2}, \tag{B.23}$$

$$K_{22\infty} = i d_{10} \int_{-\infty}^{\infty} \frac{\alpha}{|\alpha|} e^{-r_1|\alpha|y} e^{-i\alpha(t-x)} d\alpha + i d_{20} \int_{-\infty}^{\infty} \frac{\alpha}{|\alpha|} e^{-r_2|\alpha|y} e^{-i\alpha(t-x)} d\alpha$$
$$= d_{10} \frac{2(t-x)}{r_1^2 y^2 + (t-x)^2} + d_{20} \frac{2(t-x)}{r_2^2 y^2 + (t-x)^2}. \tag{B.24}$$

Taking the limit as $y \to 0$, Eqs. (B.21–B.24) become

$$K_{11\infty} = \lim_{y\to 0} \left[a_{10} \frac{2(t-x)}{r_1^2 y^2 + (t-x)^2} + a_{20} \frac{2(t-x)}{r_2^2 y^2 + (t-x)^2} \right] = \frac{2a_0}{t-x}, \tag{B.25}$$

$$K_{21\infty} = \lim_{y\to 0} \left[b_{10} \frac{2y}{r_1^2 y^2 + (t-x)^2} + b_{20} \frac{2y}{r_2^2 y^2 + (t-x)^2} \right] = 2b_0 \pi \delta(t-x) \tag{B.26}$$

$$K_{12\infty} = \lim_{y\to 0} \left[c_{10} \frac{2y}{r_1^2 y^2 + (t-x)^2} + c_{20} \frac{2y}{r_2^2 y^2 + (t-x)^2} \right] = 2c_0 \pi \delta(t-x) \tag{B.27}$$

$$K_{22\infty} = \lim_{y\to 0} \left[d_{10} \frac{2(t-x)}{r_1^2 y^2 + (t-x)^2} + d_{20} \frac{2(t-x)}{r_2^2 y^2 + (t-x)^2} \right] = \frac{2d_0}{t-x}. \tag{B.28}$$

For the rest of the terms in the asymptotic expansion, the reader is referred to [62].

Appendix C: Functions appearing in the integral equations (21)

$$\omega_1 = \frac{c_0}{a_0}, \tag{C.1}$$

$$\omega_2 = -\frac{b_0}{d_0}, \tag{C.2}$$

$$\lambda_1 = -\frac{1}{2a_0}, \tag{C.3}$$

$$\lambda_2 = -\frac{1}{2d_0}, \tag{C.4}$$

where a_0, b_0, c_0, d_0 are given in Appendix B;

$$J_{11}(t,x) = -\frac{1}{a_0}\int_0^\infty \Phi_{11}(\alpha)\sin[\alpha(t-x)]\,\mathrm{d}\alpha, \tag{C.5}$$

$$J_{21}(t,x) = -\frac{1}{d_0}\int_0^\infty \Phi_{21}(\alpha)\cos[\alpha(t-x)]\,\mathrm{d}\alpha, \tag{C.6}$$

$$J_{12}(t,x) = -\frac{1}{a_0}\int_0^\infty \Phi_{12}(\alpha)\cos[\alpha(t-x)]\,\mathrm{d}\alpha, \tag{C.7}$$

$$J_{22}(t,x) = -\frac{1}{d_0}\int_0^\infty \Phi_{22}(\alpha)\sin[\alpha(t-x)]\,\mathrm{d}\alpha, \tag{C.8}$$

$$\Phi_{11}(\alpha) = -\frac{\alpha}{\Delta_0(\alpha)}\left[\frac{(1-\nu^2)}{2}\left(\bar{Z}_2(\alpha)+Z_2(\alpha)\right)\right] - a_0\frac{\alpha}{|\alpha|}, \tag{C.9}$$

$$\Phi_{21}(\alpha) = -\frac{i\alpha}{\Delta_0(\alpha)}\left[\frac{(1-\nu^2)}{2}\left(A_2\bar{Z}_2(\alpha)-\bar{A}_2Z_2(\alpha)\right)\right] - b_0, \tag{C.10}$$

$$\Phi_{12}(\alpha) = \frac{i\alpha}{\Delta_0(\alpha)}\left[(\kappa+\nu)\left(-\bar{Z}_1(\alpha)+Z_1(\alpha)\right)\right] - c_0, \tag{C.11}$$

$$\Phi_{22}(\alpha) = \frac{\alpha}{\Delta_0(\alpha)}\left[(\kappa+\nu)\left(-A_2(\alpha)\bar{Z}_1(\alpha)-\bar{A}_2(\alpha)Z_1(\alpha)\right)\right] - d_0\frac{\alpha}{|\alpha|}. \tag{C.12}$$

References

1. Mindlin, R.D.: Compliance of elastic bodies in contact. J. Appl. Mech. **16**, 259–268 (1949)
2. Sneddon, I.N.: Fourier Transforms. McGraw-Hill, New York (1951)
3. Muskhelishvili, N.I.: Some Basic Problems of the Mathematical Theory of Elasticity. Noordhoff, Groningen (1953)
4. Spence, D.A.: The Hertz problem with finite friction. J. Elast. **5**, 297–319 (1975)
5. Keer, L.M., Mowry, D.B.: The stress field created by a circular sliding contact on transversely isotropic spheres. Int. J. Solids Struct. **15**, 33–39 (1979)
6. Gladwell, G.M.L.: Contact Problems in the Classical Theory of Elasticity. Sijtho and Noordho, Alphen aan den Rijn (1980)
7. Johnson, K.L.: Contact Mechanics. Cambridge University Press, London (1985)
8. Hills, D.A., Nowell, D., Sackfield, A.: Mechanics of Elastic Contact. Butterworth-Heinemann, Oxford (1993)
9. Barber, J.R.: Elasticity, 3rd edn. Springer, Berlin (2009)
10. Barber, J.R., Ciavarella, M.: Contact mechanics. Int. J. Solids Struct. **37**, 29–43 (2000)
11. Giannakopoulos, A.E., Pallot, P.: Two-dimensional contact analysis of elastic graded materials. J. Mech. Phys. Solids **48**, 1597–1631 (2000)
12. Guler, M.A., Erdogan, F.: Contact mechanics of graded coatings. Int. J. Solids Struct. **41**, 3865–3889 (2004)
13. Ke, L.L., Wang, Y.S.: Two-dimensional contact mechanics of functionally graded materials with arbitrary spatial variations of material properties. Int. J. Solids Struct. **43**, 5779–5798 (2006)
14. Dag, S., Guler, M.A., Yildirim, B., Ozatag, A.C.: Sliding frictional contact between a rigid punch and a laterally graded elastic medium. Int. J. Solids Struct. **46**, 4038–4053 (2009)
15. Guler, M.A.: Contact Mechanics of FGM Coatings: An Integral Equation Approach. VDM Verlag, Saarbrücken (2009)
16. Choi, H.J., Paulino, G.H.: Thermoelastic contact mechanics for a flat punch sliding over a graded coating/substrate system with frictional heat generation. J. Mech. Phys. Solids **56**, 1673–1692 (2008)
17. Ke, L.L., Wang, Y.S., Yang, J.: Sliding frictional contact analysis of functionally graded piezoelectric layered half-plane. Acta Mech. **209**, 249–268 (2010)
18. Chen, P., Chen, S.: Contact behaviors of a rigid punch and a homogeneous half-space coated with a graded layer. Acta Mech. **223**, 563–577 (2012)
19. Chen, P.J., Chen, S.H.: Thermo-mechanical contact behavior of a finite graded layer under a sliding punch with heat generation. Int. J. Solids Struct. **50**, 1108–1119 (2013)
20. Chen, P.J., Chen, S.H.: Partial slip contact between a rigid punch with an arbitrary tip-shape and an elastic graded solid with finite thickness. Mech. Mater. **59**, 24–35 (2013)
21. Giannakopoulos, A.E., Pallot, P.: Two-dimensional contact analysis of elastic graded materials. J. Mech. Phys. Solids **48**, 1597–1631 (2000)

22. Chen, S.H., Yan, C., Soh, A.: Adhesive behavior of two-dimensional power-law graded materials. Int. J. Solids Struct. **46**, 3398–3404 (2009)
23. Chen, S.H., Yan, C., Zhang, P., Gao, H.J.: Mechanics of adhesive contact on a power-law graded elastic half-space. J. Mech. Phys. Solids **57**, 1437–1448 (2009)
24. Green, A.E., Zerna, W.: Theoretical Elasticity. Oxford University Press, Oxford (1954)
25. Leknitskii, S.G.: Theory of Elasticity of an Anisotropic Elastic Body. Holden-Day, San Francisco (1963)
26. Sveklo, V.A.: Boussinesq type problems for the anisotropic half-space. PMM **28**, 908–913 (1964)
27. Turner, J.R.: Contact on a transversely isotropic half-space, or between two transversely isotropic bodies. Int. J. Solids Struct. **16**, 409–419 (1966)
28. Willis, J.R.: Hertzian contact of anisotropic bodies. J. Mech. Phys. Solids **14**, 163–176 (1966)
29. Dahan, M., Zarka, J.: Elastic contact between a sphere and a semi infinite transversely isotropic body. Int. J. Solids Struct. **13**, 229–238 (1977)
30. Hwu, C., Fan, C.W.: Solving the punch problems by analogy with the interface crack problems. Int. J. Solids Struct. **35**, 3945–3960 (1998)
31. Pan, E., Yuan, F.: Three-dimensional Green's functions in anisotropic bimaterials. Int. J. Solids Struct. **37**, 5329–5351 (2000)
32. Pan, E.: Three-dimensional Green's functions in anisotropic magneto-electro-elastic bimaterials. Z. Angew. Math. Phys. **53**, 815–838 (2002)
33. Pan, E., Yang, B.: Three-dimensional interfacial Green's functions in anisotropic bimaterials. Appl. Math. Model. **27**, 307–326 (2003)
34. Borodich, F.: Some contact problems of anisotropic elastodynamics: integral characteristics and exact solutions. Int. J. Solids Struct. **37**, 3345–3373 (2000)
35. Ciavarella, M., Demelio, G., Schino, M., Vlassak, J.J.: The general 3D Hertzian contact problem for anisotropic materials. Key Eng. Mater. **221**, 281–292 (2001)
36. Barnett, D., Lothe, J.: Line force loadings on anisotropic half-spaces and wedges. Phys. Nor. **8**, 13–22 (1975)
37. Shi, D., Lin, Y., Ovaert, T.C.: Indentation of an orthotropic half-space by a rigid ellipsoidal indenter. J. Tribol. Trans. ASME **125**, 223–231 (2003)
38. Swanson, S.R.: Hertzian contact of orthotropic materials. Int. J. Solids Struct. **41**, 1945–1959 (2004)
39. Willis, J.R.: Hertzian contact of anisotropic bodies. J. Mech. Phys. Solids **14**, 163–176 (1966)
40. Pagano, N.J.: Exact solutions for rectangular bidirectional composites and sandwich plates. J. Compos. Mater. **4**, 20–34 (1970)
41. Srinivas, S., Rao, A.K.: Bending, vibration and buckling of simply supported thick orthotropic rectangular plates and laminates. Int. J. Solids Struct. **6**, 1463–1481 (1970)
42. Lin, Y., Ovaert, T.: A rough surface contact model for general anisotropic materials. J. Tribol. **126**, 41–49 (2004)
43. Rand, O., Rovenskii, V.: Analytical Methods in Anisotropic Elasticity: With Symbolic Computational Tools. Birkhauser, Basel (2005)
44. Ning, X., Lovell, M.R., Slaughter, W.S.: Asymptotic solutions for axisymmetric contact of a thin, transversely isotropic elastic layer. Wear **260**, 693–698 (2006)
45. Li, X., Wang, M.: Hertzian contact of anisotropic piezoelectric bodies. J. Elast. **84**, 153–166 (2006)
46. Ramirez, G.: Frictionless contact in a layered piezoelectric medium characterized by complex eigenvalues. Smart Mater. Struct. **15**, 1287–1295 (2006)
47. Galin, L.: Contact Problems: The Legacy of LA Galin. Springer, Berlin (2008)
48. He, L., Ovaert, T.: Three-dimensional rough surface contact model for anisotropic materials. J. Tribol. **130**, 021402-1–021402-6 (2008)
49. Batra, R.C., Jiang, W.: Analytical solution of the contact problem of a rigid indenter and an anisotropic linear elastic layer. Int. J. Solids Struct. **45**, 5814–5830 (2008)
50. Jiang, W., Batra, R.C.: Indentation of a laminated composite plate with an interlayer rectangular void. Compos. Sci. Technol. **70**, 1023–1030 (2010)
51. Erbas, B., Yusufoglu, E., Kaplunov, J.: A plane contact problem for an elastic orthotropic strip. J. Eng. Math. **70**, 399–409 (2011)
52. Zhou, Y.T., Lee, K.Y.: Exact solutions of a new, 2D frictionless contact model for orthotropic piezoelectric materials indented by a rigid sliding punch. Philos. Mag. A **92**, 1937–1965 (2012)
53. Bagault, C., Nélias, D., Baietto, M.C.: Contact analyses for anisotropic half space: effect of the anisotropy on the pressure distribution and contact area. J. Tribol. **134**, 031401–10314018 (2012)
54. Bagault, C., Nélias, D., Baietto, M.C., Ovaert, T.C.: Contact analyses for anisotropic half-space coated with an anisotropic layer: effect of the anisotropy on the pressure distribution and contact area. Int. J. Solids Struct. **50**, 743–754 (2013)
55. Blazquez, A., Mantic, V., Pars, F.: Application of BEM to generalized plane problems for anisotropic elastic materials in presence of contact. Eng. Anal. Bound. Elem. **30**, 489–502 (2006)
56. Rodríguez-Tembleque, L., Buroni, F.C., Abascal, R., Sáez, A.: 3D frictional contact of anisotropic solids using BEM. Eur. J. Mech. A Solids **30**, 95–104 (2011)
57. Guler, M.A.: Contact stresses in an orthotropic medium: a closed-form solution. Int. J. Mech. Sci. **87**, 72–88 (2014)
58. Kucuksucu, A., Guler, M.A., Avci, A.: Closed-form solution of a frictional sliding contact problem for an orthotropic elastic half-plane indented by a wedge-shaped punch. Key Eng. Mater. **618**, 203–225 (2014)
59. Bakırtaş, I.: The contact problem of an orthotropic non-homogeneous elastic half-space. Int. J. Eng. Sci. **22**, 347–359 (1984)
60. Krenk, S.: On the elastic constants of plane orthotropic elasticity. J. Compos. Mater. **13**, 108–116 (1979)
61. Cinar, A., Erdogan, F.: The crack and wedging problem for an orthotropic strip. Int. J. Fract. **19**, 83–102 (1983)
62. Kucuksucu, A.: Contact Mechanics Analysis of Orthotropically Graded Materials. Ph.D.Dissertation. Mechanical Engineering Department, Selçuk University, Konya, Turkey (2011)
63. Erdogan, F.: Mixed boundary value problems in mechanics. In: Nemat-Nasser, S. (ed.) Mechanics Today, vol. 4, pp 1–86. Pergamon Press, Oxford (1978)
64. Erdogan, F., Gupta, G.D.: On the numerical solution of singular integral equations. Q. Appl. Math. **29**, 525–534 (1972)

65. Ozturk, M., Erdogan, F.: Mode I crack problem in an inhomogeneous orthotropic medium. Int. J. Eng. Sci. **35**, 869–883 (1997)
66. Ozturk, M., Erdogan, F.: The mixed mode crack problem in an inhomogeneous orthotropic medium. Int. J. Fract. **98**, 243–261 (1999)
67. Guler, M.A.: The Problem of a Rigid punch with Friction on a Graded Elastic Medium. MS Thesis, Mechanical Engineering Department, Lehigh University, Bethlehem (1996)
68. Elloumi, R., Guler, M.A., Kallel-Kamoun, I., El-Borgi, S.: Closed-form solutions of the frictional sliding contact problem for a magneto-electro-elastic half-plane indented by a rigid conducting punch. Int. J. Solids Struct. **50**, 3778–3792 (2013)
69. Elloumi, R., Kallel-Kamoun, I., El-Borgi, S., Guler, M.A.: On the frictional sliding contact problem between a rigid circular conducting punch and a magneto-electro-elastic half-plane. Int. J. Mech. Sci. **87**, 1–17 (2014)